

Holographic RG flows in a 3d gauged supergravity at finite temperature

Anastasia Golubtsova^{1, a, b}, Alexander Nikolaev^{2, b, c}, Mikhail Podoinitsyn^{3, a}

(a) *Bogoliubov Laboratory of Theoretical Physics, JINR,
Joliot-Curie str. 6, Dubna, 141980 Russia*

(b) *Steklov Mathematical Institute, Russian Academy of Sciences
Gubkina str. 8, 119991 Moscow, Russia*

(c) *Physics Department, Lomonosov Moscow State University, 1-2 Leninskie Gory,
Moscow 119991, Russia*

Abstract

In this paper we consider finite-temperature holographic RG flows in $D = 3$ $\mathcal{N} = (2, 0)$ gauged truncated supergravity coupled to a sigma model with a hyperbolic target space. In the context of the holographic duality, fixed points (CFTs) at finite temperature are described by AdS black holes. We come from the gravity EOM to a 3d autonomous dynamical system, which critical points can be related to fixed points of dual field theories. Near-horizon black hole solutions correspond to infinite points of this system. We use Poincaré transformations to project the system on \mathbf{R}^3 into the 3d unit cylinder such that the infinite points are mapped onto the boundary of the cylinder. We explore numerically the space of solutions. We show that the exact RG flow at zero temperature is the separatrix for asymptotically AdS black hole solutions if the potential has one extremum, while for the potential with three extrema the separatrices are RG flows between AdS fixed points. We find near-horizon analytical solutions for asymptotically AdS black holes using the dynamical equations. We also present a method for constructing full analytical solutions.

Contents

| | | |
|----------|----------------------------------------------|----------|
| 1 | Introduction | 3 |
| 2 | Setup | 6 |
| 2.1 | The supergravity model | 6 |
| 2.2 | The scalar field near the boundary | 9 |
| 2.3 | Autonomous dynamical system | 10 |

¹golubtsova@theor.jinr.ru

²alex99@gmail.com

³mpod@theor.jinr.ru

| | | |
|----------|-------------------------------------------------------------------------|-----------|
| 3 | Global structure of solutions | 12 |
| 3.1 | Dynamics on a 2d Poincaré disk | 12 |
| 3.2 | Compactified 3d autonomous system and its critical sets | 17 |
| 3.3 | Flows of the 3d autonomous system in the unit cylinder | 20 |
| 3.3.1 | The case $a^2 < 1/2$ | 21 |
| 3.3.2 | The case $1/2 < a^2 < 1$ | 21 |
| 4 | Near-horizon solutions from the dynamical system | 27 |
| 4.1 | Qualitative analysis of critical points at finite temperature | 27 |
| 4.2 | Reconstruction of asymptotic solutions near critical points | 29 |
| 4.3 | Generalization for an arbitrary ϕ_h | 32 |
| 5 | Improved near-horizon solutions for the scalar field | 35 |
| 6 | Conclusions | 37 |
| A | Exact holographic RG flow | 39 |
| B | AdS black hole solutions | 39 |
| B.1 | Exact solutions | 39 |
| B.2 | Near-horizon solutions | 40 |
| C | Fixed points and holographic RG flows at $T = 0$ | 42 |
| C.1 | Stability of the critical points | 42 |
| C.2 | Holographic RG flows at zero temperature | 43 |

1 Introduction

The notion of renormalization group [1, 2]- [6] gives a unified approach to the systems with many degrees of freedom. Fixed points of the renormalization group equations are conformal field theories, which are connected by RG flows. RG flows can be induced either by an operator deformation of the original CFT, or by an operator VEV.

Holographic duality provides a map between d -dimensional quantum field theories at strongly coupling and weakly coupled $(d + 1)$ -dimensional gravity [7–9]. This map is furnished by calculations of observables from both sides. This procedure yields a technical difficulty, namely, both field and gravity sides suffer from infinities, that can be observed, for example, from calculations of two-point correlation functions [10]. One needs to perform the renormalization procedure to remove divergences systematically and consistently.

In [11] it was found that equations of motion of Type IIB supergravity on $AdS_5 \times S^5$ can be associated with renormalization group flow equations of the dual gauge theory. In the holographic prescription RG flow [12–14] are described in terms of gravitational domain wall solutions with AdS boundaries and certain boundary conditions for the field content [14–16]. The extrema of the scalar potential are in a one-to-one correspondence with fixed points of RG flows, thus typically maxima of the potential are related with UV fixed points, and minima with IR fixed points. While the boundaries of the domain wall solutions can be related with fixed points of RG flow (CFTs) of dual field theories, the solutions themselves with certain boundary conditions can be interpreted as deformations of fixed points either by relevant operators or by non-zero vacuum expectation values of operators [17]- [21].

In the extrema of the scalar potential the gravity solutions are AdS spacetimes, so as, it was said above, the holographic RG flows correspond to gravity solutions, which are asymptotically AdS. However, there can be an additional case, namely, when the scalar potential can have only one extreme point, this can be the case for supergravity actions after reduction from higher dimensions or truncation. Then the flow can run from the extremum of the potential to infinity as the scalar field diverges, $\phi \rightarrow \pm\infty$. The corresponding geometry of the critical point is just scale-invariant and doesn't possess conformal invariance¹. Such solutions are singular since the divergence of the scalar field and the potential leads to the divergence of curvature invariants of the metrics. However, such solutions can be acceptable in holography, if the Gubser's bound [22] and/or a criterion of spectral computability is satisfied. A classification of holographic RG flows at zero temperature was given in [23], where exotic RG flows including those with bounces and skipping RG flows were also discussed.

To study thermal properties of QFT it is of interest to explore a generalization of holographic RG flows to finite temperature. The analysis of holographic RG flows at finite temperature allows to find out the consistence of the theory. From the gravity side, fixed points at finite temperature are described by AdS black holes. Thus, the domain wall solution is replaced by a black hole (brane) written in the domain wall coordinates.

In [24, 25] holographic thermal RG flows were studied to clarify properties of exotic RG flows using the holographic approach. Holographic RG flows with finite-temperature corresponding generalizations were investigated in works [26–31] for applications to bottom-up models of holographic QCD.

¹In what follows we refer to them as scaling solutions.

In this paper we consider fixed points of holographic RG flows at finite temperature for $D = 3$ $\mathcal{N} = 2$ gauged supergravity coupled to a sigma model with a hyperbolic target space $\mathbb{H}^2 = \frac{SU(1,1)}{U(1)}$ [32, 33]. The supergravity model is truncated, such that we deal with a model of dilaton gravity, which scalar potential has either a single extremum defined at the origin or three extrema depending to the value of the target space curvature. Note that the vacuum at the origin of the potential is supersymmetric, while two additional are not. Holographic RG flows at zero temperature for this model were studied in [33–35]. An exact half-supersymmetric holographic RG flow interpolating between AdS_3 and scaling geometries was found in [33]. Despite this RG flow has a singularity as $\phi \rightarrow \infty$, the solution satisfies Gubser’s bound for the case of the negatively defined scalar potential with a single extremum. In [35] extending previous works [33, 34] holographic RG flows for the model were discussed choosing different boundary conditions for the field content.

Our primary interest will be black hole solutions which asymptote to fixed points of the holographic RG flows at zero temperature from [34, 35]. As in these works we come from the equations of motion for the holographic model to a 3d system of a first-order autonomous dynamical system. This can be considered as an interpretation of RG flows of the dual CFT as the dynamical system [36], such that RG flows are certain trajectories in the phase space. Zero-temperature holographic RG flows with Dirichlet boundary conditions have fixed points, which are equilibria of this system and related with the maximum and minima of the scalar potential of the model, correspond to UV CFT and IR CFTs, respectively. These fixed points of the system have different types of the dynamical stability. For the scalar potential with a single critical point RG flows with Dirichlet boundary conditions have a UV conformal fixed point at the origin and IR scaling fixed points as the potential goes to infinity. Infinite points of this system are related with black hole solutions near horizon.

We apply Poincaré transformations [38–40] to compactify the phase space of the system into the unit cylinder, such that the infinite points are projected on its boundary. Thus, near-horizon regions of asymptotically AdS black holes are mapped on the critical line of the system on the boundary of the cylinder. Note, that near-horizon regions of black holes as infinite points of autonomous dynamical systems, which have origin from some gravity models were considered in works [41, 42]. The authors used Poincaré transformations to project the phase space of the gravitational dynamical system into the ball to explore infinite points of the equations of motion and, then, estimate asymptotic black hole solutions.

We solve numerically the equations to find black hole solutions starting from near-horizon regions and ending at AdS zero-temperature fixed points. To analyze the numerical solutions, we also construct the known exact RG flow and AdS black hole solutions in the phase space, that helps us to understand the global phase portrait of the system. The construction and analysis of the solutions is similar to [28, 37]. For the negatively defined scalar potential with one extremum the black hole solutions tending to the AdS fixed point pass very close near the curve of the exact RG flow. Thus, this is a separatrix for the asymptotically AdS black hole solutions. However, for the solutions corresponding to the potential with two additional minima this no longer holds. For this case separatrices for the asymptotically AdS black hole solutions are the flows, which connects the AdS fixed points at the maximum and minima of the potential and dual to different CFTs. From the point of view of the dynamical system holographic RG flows at zero temperature are trajectories between certain critical points, while in the thermal case RG flows are hypersurfaces, which one of the boundaries is a

separatrix for asymptotically AdS black hole solutions with different ϕ_h .

While to construct the full analytic black hole solutions with AdS asymptotics is quite difficult, we are able to find a description for the near-horizon region. The solutions are characterized by the value of the scalar field at the horizon ϕ_h and can be divided into two classes: 1) when ϕ_h matches with a value of the critical point of the scalar potential and 2) when ϕ_h is located between of the critical points of the potential or between the critical point and the zero of the potential.

For flows starting near the maximum of the scalar potential, we are able to improve the analytical black hole solutions in sense that the solutions can be extended to the boundary as well. In this work we restrict ourselves to the solution for the scalar field as a function of the scale factor.

The paper is organized as follows. In section 2 we give a setup: we review the holographic model and derive the 3d autonomous dynamical system from the equations of motion. In section 3 using Poincaré transformation we project the system into the unit cylinder, that provides us to understand the global phase portrait and construct the flows numerically. We analyze the behaviour of the flows from the near-horizon regions to the boundaries. In section 4 we construct analytic near-horizon black hole solutions. In section 5 we find a generalization of the solutions for the scalar field obtained in the previous section, which are valid for the region near the boundary. We finish with further discussion in section 6. Some technical details are left for Appendices.

2 Setup

2.1 The supergravity model

The gravity model of our interest is $\mathcal{N} = (2, 0)$ AdS₃ supergravity with n -copies of $\mathcal{N} = (2, 0)$ scalar multiplet designed in [32]. The field content includes a vielbein e_μ^a , a gravitini ψ_μ and a gauge field A_μ . The scalar multiplet consists of a complex scalar field Φ and by a doublet of spinorial fields λ . In the work [32] the generic case where scalars parametrize a coset space G/H was discussed with a compact or non-compact G and its maximal compact subgroup H . In this paper, as in [34, 35], we focus on the non-compact case for G with a single complex scalar field Φ , so the coset space is $\frac{SU(1,1)}{U(1)} = \mathbb{H}^2$.

The bosonic part of the Lagrangian [32] reads

$$e^{-1}\mathcal{L} = \frac{1}{4}R - \frac{e^{-1}}{16m a^4}\epsilon^{\mu\nu\rho}A_\mu\partial_\nu A_\rho - \frac{|D_\mu\Phi|^2}{a^2(1-|\Phi|^2)} - V(\Phi), \quad (2.1)$$

where we define $e = \det e_\mu^a$, $D_\mu\Phi = (\partial_\mu + iA_\mu)\Phi$ and $-4m^2$ is the AdS₃ cosmological constant. The parameter a is related to the curvature of the scalar manifold and should be non-zero². The potential $V(\Phi)$ in (2.1) is given by

$$V(\Phi) = 2m^2C^2(2a^2|S|^2 - C^2), \quad (2.2)$$

where

$$C = \frac{1+|\Phi|^2}{1-|\Phi|^2}, \quad S = \frac{2\Phi}{1-|\Phi|^2}. \quad (2.3)$$

Introducing the following redefinition of the scalar field

$$C \equiv \cosh \phi, \quad |S| \equiv \sinh \phi \quad (2.4)$$

allows us to rewrite the kinetic term of the scalar field in the standard form, i.e. the Lagrangian (2.1) comes to

$$e^{-1}\mathcal{L} = \frac{1}{4}R - \frac{e^{-1}}{a^4}\epsilon^{\mu\nu\rho}A_\mu\partial_\nu A_\rho - \frac{1}{4a^2}\partial_\mu\phi\partial^\mu\phi - \frac{1}{4a^2}|S|^2(\partial_\mu\theta + A_\mu)(\partial^\mu\theta + A^\mu) - V(\phi). \quad (2.5)$$

Switching off θ and the vector field A_μ , $A_\mu = \theta = 0$, which is a consistent truncation of the theory, one finally comes to the action

$$S = \frac{1}{16\pi G_3} \int d^3x \sqrt{|g|} \left(R - \frac{1}{a^2}(\partial\phi)^2 - V(\phi) \right) + \frac{1}{8\pi G_3} \int_{\partial M} d^2x \sqrt{|\gamma|} K, \quad (2.6)$$

where the potential $V(\phi)$ is given by:

$$V(\phi) = 2\Lambda_{uv} \cosh^2 \phi [(1 - 2a^2) \cosh^2 \phi + 2a^2], \quad (2.7)$$

where $\Lambda_{uv} = -4m^2$.

²The $a = 0$ case corresponds to the flat sigma model.

The GHY term in (2.6) includes the determinant of the induced metric γ on the boundary ∂M and the extrinsic curvature K

$$K = \gamma^{\mu\nu} K_{\mu\nu}, \quad K_{\mu\nu} = -\nabla_\mu n_\nu = \frac{1}{2} n^\rho \partial_\rho \gamma_{\mu\nu}, \quad n^\mu = \frac{\delta_w^\mu}{\sqrt{g_{ww}}}. \quad (2.8)$$

We show the behaviour of the potential on the scalar field in Fig. 1. Note that for $a^2 \leq \frac{1}{2}$ and for $a^2 \geq 1$ the potential has one extremum, namely,

$$\phi_1 = 0, \quad (2.9)$$

while for $\frac{1}{2} < a^2 < 1$ the potential has two more extremal points, i.e.

$$\phi_{2,3} = \frac{1}{2} \ln \left(\frac{1 \pm 2|a|\sqrt{1-a^2}}{2a^2-1} \right). \quad (2.10)$$

Moreover, if we consider the case $a^2 > \frac{1}{2}$ the scalar potential has also zeroes:

$$\phi_\pm = \pm \cosh^{-1} \left(\frac{a}{\sqrt{a^2 - \frac{1}{2}}} \right). \quad (2.11)$$

The behavior of the potential V on ϕ for various a is presented in Figs. 1. We marked by ϕ_3 and ϕ_2 (2.10) the left and right extrema of the potential, correspondingly.

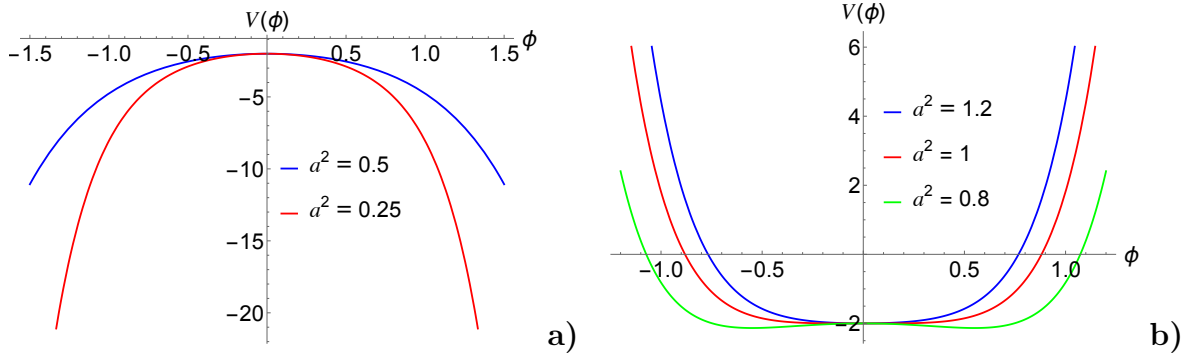


Figure 1: The potential (2.7) against the scalar field ϕ for different values of a . For all we set $\Lambda_{uv} = -1$.

In this work we restrict ourselves to the cases 1) $a^2 \leq \frac{1}{2}$ and 2) $\frac{1}{2} < a^2 < 1$. The potential is related to the superpotential through the equation

$$V = \frac{a^2}{4} W'^2 - \frac{1}{2} W^2. \quad (2.12)$$

The exact supersymmetric solution for W from eq. (2.12) has the following form

$$W_{\text{susy}} = -\cosh^2 \phi. \quad (2.13)$$

Note, that eq.(2.12) has other solutions, which, however, cannot be obtained from the supersymmetric variations of the model, comparing to (2.13). Below we will call such solutions to (2.12) as fake superpotentials.

The generic form of the stress-energy tensor for (2.6) reads as follows

$$T_{\mu\nu} = \frac{1}{a^2} \left(\partial_\mu \phi \partial_\nu \phi - \frac{1}{2} g_{\mu\nu} \partial_\sigma \phi \partial^\sigma \phi \right) - \frac{1}{2} g_{\mu\nu} V. \quad (2.14)$$

To study a black hole solution for the model (2.6) we consider the following ansatz of the metric in the domain wall coordinates

$$ds^2 = e^{2A(w)} \left(-f(w) dt^2 + dx^2 \right) + \frac{dw^2}{f(w)}, \quad (2.15)$$

where the radial coordinate runs the region $w \in (w_h, +\infty)$, with a location of the horizon w_h and the conformal boundary at $w \rightarrow +\infty$. In (2.15) $A = A(w)$ is the scale factor, the function $f(w)$ is increasing on (w_h, ∞) and defined the position of the horizon

$$f(w) \approx \begin{cases} 1, & \text{if } w \rightarrow +\infty. \\ 0, & \text{if } w \rightarrow w_h. \end{cases} \quad (2.16)$$

The temperature of the solution (2.15) can be found as

$$T_H = \frac{e^{A(w_h)}}{4\pi} \left| \frac{df}{dw} \right|_{w=w_h}. \quad (2.17)$$

The Hawking temperature (2.17) of the black hole (2.15) corresponds to the temperature of the dual field theory.

For the scalar field we also choose the dependence only on the radial coordinate w

$$\phi = \phi(w). \quad (2.18)$$

We suppose that the scalar field takes some finite value at the horizon w_h

$$\phi(w_h) = \phi_h. \quad (2.19)$$

Holographic RG flows and its fixed points for the gravity model (2.6)-(2.7) with an ansatz of the metric without a black hole, i.e. for (2.15) with $f = 1$, was studied in [34, 35].

In what follows it is convenient to introduce the function

$$g = \ln f. \quad (2.20)$$

Then the Einstein equations to (2.6) can be written down as follows

$$2\ddot{A} + 2\dot{A}^2 + \dot{A}\dot{g} + e^{-g}V + \frac{\dot{\phi}^2}{a^2} = 0, \quad (2.21)$$

$$3\dot{A}\dot{g} + 2\ddot{A} + 2\dot{A}^2 + \dot{g}^2 + \ddot{g} + e^{-g}V + \frac{\dot{\phi}^2}{a^2} = 0, \quad (2.22)$$

$$\dot{A}\dot{g} + 2\dot{A}^2 + e^{-g}V - \frac{\dot{\phi}^2}{a^2} = 0, \quad (2.23)$$

where we denote by dot the derivative with respect the radial coordinate w . The scalar field equation can be represented as

$$\square\phi = \frac{a^2}{2}V_\phi, \quad \square = \frac{1}{\sqrt{|g|}}\partial_\mu\left(g^{\mu\nu}\sqrt{|g|}\partial_\nu\right) = e^{-2A}\partial_w\left(f(w)e^{2A}\partial_w\right), \quad (2.24)$$

or

$$\dot{g}\dot{\phi} + 2\dot{A}\dot{\phi} + \ddot{\phi} - \frac{a^2}{2}e^{-g}V_\phi = 0, \quad (2.25)$$

where V_ϕ is a derivative of the scalar potential with respect to the scalar field.

For values ϕ_h of the scalar field ϕ such that, such that $V_\phi(\phi_h) = 0$ (i.e. $\phi_h = \phi_{1,2,3}$) the equations (2.21)-(2.25) enjoy the exact AdS black hole solution (see e.g. [24])

$$A(w) = \sqrt{-\frac{V(\phi_h)}{2}}w, \quad f(w) := e^{g(w)} = 1 - e^{-\sqrt{-2V(\phi_h)}(w-w_h)}, \quad (2.26)$$

where $V(\phi_h)$ is the value of the potential at the extremum and the conformal boundary corresponds to the radial coordinate tending to infinity $w \rightarrow +\infty$. Similar to pure AdS solutions we have only one AdS black hole at $\phi = \phi_1$ for $a^2 \leq \frac{1}{2}$, while for $\frac{1}{2} < a^2 < 1$ we have three AdS black hole solutions for different extrema of the scalar potential, i.e. at $\phi = \phi_{1,2,3}$.

Note, that for $f = 1$ the model has an exact half-supersymmetric solution, which interpolates between AdS ans scaling geometries [33]. We briefly discuss it in Appendix A.

2.2 The scalar field near the boundary

The scalar potential V (2.7) near the extremum $\phi = \phi_1$ has the following expansion up to the quadratic order

$$V = -2m^2 + 4m^2(a^2 - 1)\phi^2 + \mathcal{O}(\phi^3), \quad (2.27)$$

while near the other extrema $\phi = \phi_{2,3}$

$$V = -\frac{2a^4m^2}{2a^2 - 1} - \frac{8a^2(a^2 - 1)m^2}{2a^2 - 1}(\phi - \phi_{2,3})^2 + \mathcal{O}(\phi^3). \quad (2.28)$$

The geometries corresponding to the extrema of the potential $\phi_{1,2,3}$ are AdS spacetimes with different radii $\ell = \sqrt{-\frac{2}{V(\phi_i)}}$ with $i = 1, 2, 3$. So we assume that the field theories dual to them are different 2d CFTs, which we call in what follows CFT_1 , CFT_2 , CFT_3 , correspondingly. They are characterized by different central charges, that can be easily seen from the Brown-Henneaux formula $c = \frac{3\ell}{2G}$.

In the regions of the extrema the solution to the equation of motion for the scalar field with (2.27) (or (2.28)) has the asymptotic form

$$\phi = \phi_- e^{-\Delta_- w} + \phi_+ e^{-\Delta_+ w}, \quad (2.29)$$

with $w \rightarrow +\infty$. In (2.29) ϕ_- and ϕ_+ are related to the source and to the VEV of the dual operator $\langle \mathcal{O} \rangle$, correspondingly.

From the scalar field equation with (2.27)-(2.28) the conformal dimensions Δ of the operators of the dual field theories are given by

$$\phi_1 : \quad \Delta_{\pm} = 1 \pm |1 - 2a^2|, \quad (2.30)$$

$$\phi_{2,3} : \quad \Delta_{\pm} = 1 \pm \sqrt{1 + \frac{8a^4(1 - a^2)}{2a^2 - 1}}. \quad (2.31)$$

The dual field theory is two-dimensional, so the operators are relevant for $\Delta < 2$, marginal for $\Delta = 2$ and irrelevant for $\Delta > 2$. The unitarity bound reads as $\Delta \geq 0$.

For ϕ_1 with $0 < a^2 < 1$: we have $1 \leq \Delta_+ < 2$ and $0 < \Delta_- < 1$, so there is an RG flow related with a deformation by a relevant operator both Δ_+ and Δ_- are driven by relevant operators.

As for $\phi_{2,3}$ the conformal dimensions Δ_{\pm} with $\frac{1}{2} < a^2 < 1$ are such that the dual operator is irrelevant $\Delta_+ > 2$ and $\Delta_- < 0$, so it breaks the unitarity bound.

The superpotential (2.12) can be expanded in series near $\phi = 0$

$$W_{\pm}(\phi) = - \left(1 + \frac{1}{2a^2} \Delta_{\pm} (\phi - \phi_*)^2 + \dots \right), \quad (2.32)$$

where the choice of the branch W_+ of W_- depends on whether the scalar field behaves near the conformal boundary as $e^{-\Delta_+ r}$ or $e^{-\Delta_- r}$ (2.29). The fake superpotential can be also represented as an expansion in series near some critical point $\phi = \phi_*$ in the following form

$$W_{\pm}(\phi) = -\sqrt{-2V_*} - \frac{1}{2a^2} \Delta_{\pm} (\phi - \phi_*)^2 + \dots, \quad (2.33)$$

with the conformal dimensions given by (2.30). Particularly, near $\phi = 0$ the fake superpotential has the form [35]

$$a^2 < \frac{1}{2} \quad \begin{cases} W_+ = -1 - \frac{1-a^2}{a^2} \phi^2 + \mathcal{O}(\phi^3), \\ W_- = -1 - \phi^2 + \mathcal{O}(\phi^3), \end{cases} \quad (2.34)$$

$$a^2 > \frac{1}{2} \quad \begin{cases} W_+ = -1 - \phi^2 + \mathcal{O}(\phi^3), \\ W_- = -1 - \frac{1-a^2}{a^2} \phi^2 + \mathcal{O}(\phi^3), \end{cases} \quad (2.35)$$

$$a^2 = \frac{1}{2}, \quad W_{\pm} = -1 - \phi^2 + \mathcal{O}(\phi^3). \quad (2.36)$$

In Appendix C.2 we give a list of possible holographic RG flows at zero temperature with different boundary conditions imposed.

2.3 Autonomous dynamical system

In this paper it is of our interest to explore holographic RG flows of the model (2.6) at finite temperature by means of the dynamical system theory. For this we represent equations of motion (2.21)-(2.23), (2.25) as an autonomous dynamical system. Then, we explore the space of the solutions to the system numerically and construct analytic black hole solutions near horizon. To come to the dynamical system, we introduce new variables [26, 28, 29]

$$X = \frac{d\phi}{dA} = \frac{\dot{\phi}}{\dot{A}}, \quad Y = \frac{dg}{dA} = \frac{\dot{g}}{\dot{A}}, \quad (2.37)$$

where $g = \ln f$, ϕ is the dilaton, A is the scale factor, and the derivatives are taken with respect to the radial coordinate w .

To parametrize the scalar field it is convenient to use the following variable:

$$z = \frac{1}{1 + e^\phi}, \quad (2.38)$$

so that $z \in [0, 1]$ for $\phi \in (-\infty; \infty)$.

Doing some algebra with eqs.(2.21)-(2.23),(2.25) we find the following useful relations

$$\frac{\ddot{g}}{\dot{A}^2} = -Y^2 - 2Y, \quad (2.39)$$

$$\frac{\ddot{A}}{\dot{A}^2} = -\frac{1}{a^2}X^2, \quad (2.40)$$

$$\frac{\ddot{\phi}}{\dot{A}^2} = -2X - XY - \frac{a^2 V_\phi}{2V} \left(2 + Y - \frac{X^2}{a^2} \right). \quad (2.41)$$

The potential and its derivative are rewritten in terms of the variable z (2.38):

$$V = \Lambda \frac{(2(z-1)z+1)^2 ((2(z-1)z+1)^2 - 2a^2(1-2z)^2)}{8(z-1)^4 z^4}, \quad (2.42)$$

$$V_\phi = \Lambda \frac{((1-2a^2)((z-1)^8 - z^8) - 2z^6(z-1)^2 + 2z^2(z-1)^6)}{2(z-1)^4 z^4}. \quad (2.43)$$

For further calculations it is convenient to define the following function

$$\mathcal{C}_{(z,a)} := \frac{a^2 V_\phi}{2V}, \quad (2.44)$$

where with (2.42)-(2.43) we have

$$\frac{V_\phi}{V} = \frac{4((1-2a^2)((z-1)^8 - z^8) - 2z^6(z-1)^2 + 2z^2(z-1)^6)}{(2(z-1)z+1)^2 ((2(z-1)z+1)^2 - 2a^2(1-2z)^2)}. \quad (2.45)$$

The function $\mathcal{C}_{(z,a)}$ (2.44) has the following zeroes

$$z_1 = \frac{1}{2}, \quad z_{2,3} = \frac{1}{2} \left(1 \mp \sqrt{\frac{1 - 3a^2 + 2\sqrt{a^2(2a^2 - 1)}}{a^2 - 1}} \right), \quad (2.46)$$

which are obviously the extrema of the potential (2.9) (2.10) in terms of the new variable z . The function (2.44) is divergent for $a^2 > 1/2$ at the points

$$z_\pm = \frac{1}{2} \left(1 \pm \sqrt{4a^2 - 2a\sqrt{4a^2 - 2} - 1} \right), \quad (2.47)$$

which correspond to the zeroes of the scalar potential (2.11)

Then the equations of motion (2.21)-(2.23),(2.25) for (2.6) are brought to the following ones

$$\frac{dz}{dA} = z(z-1)X, \quad (2.48)$$

$$\frac{dX}{dA} = \left(\frac{X^2}{a^2} - Y - 2 \right) (X + \mathcal{C}_{(z,a)}), \quad (2.49)$$

$$\frac{dY}{dA} = Y \left(\frac{X^2}{a^2} - Y - 2 \right). \quad (2.50)$$

The equilibrium points are defined by zeros of the LHS of the system (2.48)-(2.50). We distinguish three cases **a)** $Y = 0$, **b)** $Y \neq 0$ and **c)** $Y \rightarrow \infty$. By virtue to (2.37) and (2.20) at the conformal boundary of the black hole spacetime $Y \rightarrow 0$, while at the horizon Y tends to infinity $Y \rightarrow \infty$. Thus only the case **c)** corresponds to finite temperature regime. The critical points with $Y = 0$ correspond to zero-temperature regime. The stability analysis of them was done in recent works [34, 35]. The corresponding geometries include both AdS and scaling spacetimes. However, only for $a^2 \leq \frac{1}{2}$ the solutions with scaling obey Gubser's bound. In Appendix C.1 we briefly review the stability of the critical points of the system at zero temperature.

In this work we are interested in fixed points of the dynamical system, which correspond to near-horizon black hole solutions, i.e. $Y \rightarrow \infty$. The exact AdS black hole geometry (2.26) can be found from eqs.(2.48)-(2.50), that is shown in Appendix B.1. To construct and analyze asymptotically AdS black holes it is more convenient to compactify the phase space. Below we apply Poincaré transformations to project the 3d dynamical system (2.48)-(2.50) defined on \mathbf{R}^3 into the unit cylinder. This helps us to explore infinite points corresponding to near-horizon black hole solutions and explore the global phase portrait of (2.48)-(2.50).

3 Global structure of solutions

In this section, we discuss the global structure of solutions for the 3d dynamical system (2.48)-(2.50). To understand the behaviour of flows at infinity we apply the so-called Poincaré projection [38–40], which maps the system into the unit cylinder. This method was used for the complete description of global phase portraits of fairly general gravitational models in works [41, 42]. Typically, Poincaré projection deals with all variables of a dynamical system mapping it onto a hemisphere (a projective plane). However, it will be more convenient for us to use the incomplete Poincaré projection (only over the variables X and Y), since the coordinate $z \in [0, 1]$ is already compact.

3.1 Dynamics on a 2d Poincaré disk

Before we give a full analysis of the 3d autonomous system, we first focus on the 2d system, which can be obtained as a slice of the system (2.48)-(2.50) for some fixed z . So the dynamics of the system is reduced to a discussion of eqs. (2.49)-(2.50) on the XY -plane, since the function $\mathcal{C}_{(z,a)}$ given by (2.44) with (2.45) tends to be constant.

The equilibrium sets of the reduced 2d dynamical system include

1. the parabola defined by the equation

$$\frac{X^2}{a^2} - Y - 2 = 0, \quad (3.1)$$

2. the point $P_0: X = -\mathcal{C}_{(z,a)}, Y = 0$ coming from

$$X + \mathcal{C}_{(z,a)} = 0. \quad (3.2)$$

The latter corresponds to pure AdS vacua if $\mathcal{C}_{z,a} = 0$. The phase portrait of eqs. (2.49)-

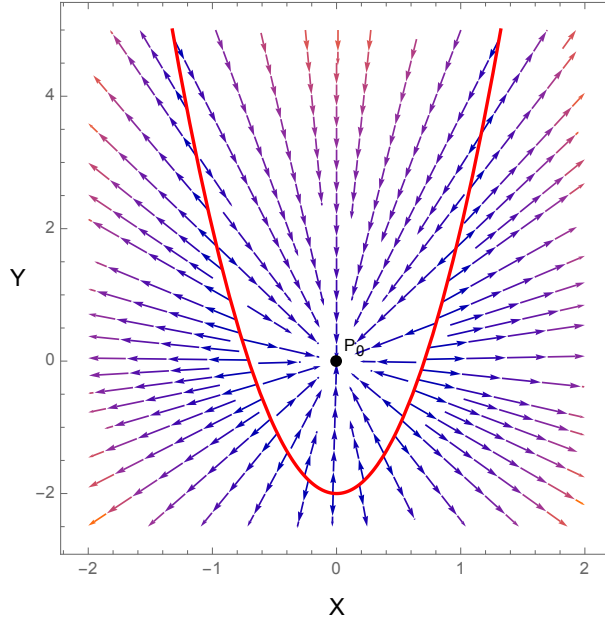


Figure 2: The flows of the dynamical system (2.49)-(2.50) at fixed z . The critical sets (the parabola and point defined by the zeroes of the RHS (2.49)-(2.50)) are shown by red. The parameters of the system a^2 and z are fixed as: $a^2 = 0.25$ and $z = 1/2$.

(2.50) with fixed z on the XY -plane is presented in Fig. 2, where the critical curve (3.1) is shown by red.

Note, the critical curve doesn't depend on z , in sense that this curve exists for each slice of $z = const$, while the location of the isolated critical point P_0 (3.2) is defined by the value of $\mathcal{C}_{(z,a)}$. The behavior of the trajectories inside the parabola in Fig. 2 is related with the position of the isolated critical point P_0 .

To extract the information about the finite temperature flows we map the system (2.49)-(2.50) defined on the plane \mathbf{R}^2 into the disc \mathbf{D}^2 . This allows to consider infinite points of eqs.(2.49)-(2.50), which are difficult to be caught considering the system on \mathbf{R}^2 .

The transformations include two parts, first, we map the dynamical system on the plane \mathbf{R}^2 onto the 2d unit sphere \mathbb{S}^2 and, then, we perform the perpendicular projection of the system on \mathbb{S}^2 into the 2d disc \mathbf{D}^2 . So we are led to study the dynamics of the system in the 2d disc \mathbf{D}^2 . To map the system on \mathbf{R}^2 (with coordinates X, Y) onto $\mathbb{S}^2 \hookrightarrow \mathbf{R}^3$

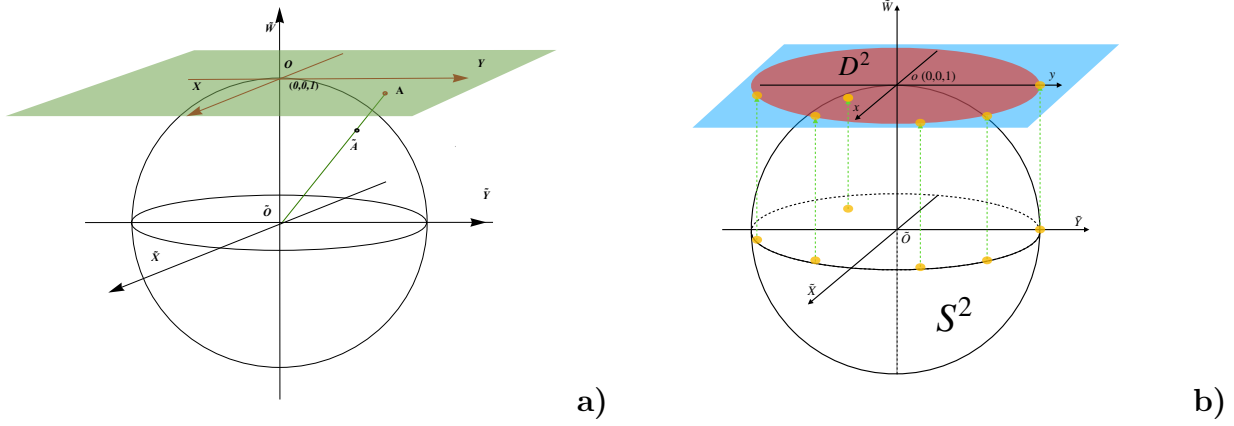


Figure 3: **a)** The Poincaré map of the plane \mathbf{R}^2 (OXY) onto the sphere \mathbb{S}^2 with coordinates $(\tilde{X}, \tilde{Y}, \tilde{W})$, where O and \tilde{O} - are the origins of the coordinates on the plane and sphere, correspondingly. The point O coincides with the north pole of the sphere \mathbb{S}^2 , i.e. its coordinates are $(0, 0, 1)$. $\tilde{A} \in \mathbb{S}^2$ is a projection of the point $A \in OXY$. **b)** The transverse map of the system from the upper hemisphere of the unit sphere \mathbb{S}^2 into the unit disk \mathbf{D}^2 . \tilde{O} is the origin of the coordinates on \mathbb{S}^2 , o is the origin of the coordinates (x, y) on \mathbf{D}^2 , that touches \mathbb{S}^2 at the point $(0, 0, 1)$. Yellow dots are images and preimages of the perpendicular projection.

(with coordinates $\tilde{X}, \tilde{Y}, \tilde{W}$) we use the Poincaré transformation ("the stereographic-like projection") given by

$$X = \frac{\tilde{X}}{\tilde{W}}, \quad Y = \frac{\tilde{Y}}{\tilde{W}}, \quad (3.3)$$

with

$$\tilde{X}^2 + \tilde{Y}^2 + \tilde{W}^2 = 1. \quad (3.4)$$

Then one can easily write down the coordinates of the new point on the sphere:

$$\tilde{X} = \frac{X}{\sqrt{X^2 + Y^2 + 1}}, \quad \tilde{Y} = \frac{Y}{\sqrt{X^2 + Y^2 + 1}}, \quad \tilde{W} = \frac{1}{\sqrt{X^2 + Y^2 + 1}}. \quad (3.5)$$

We suppose that the plane \mathbf{R}^2 , where the system (2.49)-(2.50) is defined, touches the sphere \mathbb{S}^2 at the north pole $(0, 0, 1)$. The points of \mathbf{R}^2 are projected onto \mathbb{S}^2 so that the points at infinity of the plane \mathbf{R}^2 come to the points on the equator of the sphere \mathbb{S}^2 , as it is shown in Fig. 3 a).

The relations (3.5) define a one-to-one correspondence between the coordinates on the plane $X, Y \in \mathbf{R}^2$ and the coordinates $(\tilde{X}, \tilde{Y}, \tilde{W})$ on the upper hemisphere of \mathbb{S}^2 , i.e. $\tilde{W} > 0$.

Then we map the system on the sphere \mathbb{S}^2 into the transverse unit disk \mathbf{D}^2 , which touches the sphere at $(0, 0, 1)$. Thus, the center of the unit disk coincides with the point, at which it contacts the plane, see Fig. 3 b). The coordinate transformations for this map are given by the following formulae:

$$\tilde{X} = x, \quad \tilde{Y} = y, \quad \tilde{W} = \sqrt{1 - x^2 - y^2}. \quad (3.6)$$

Consequently, the system on the plane \mathbf{R}^2 is projected into the disk by the coordinate transformations

$$X = \frac{x}{\sqrt{1-x^2-y^2}}, \quad Y = \frac{y}{\sqrt{1-x^2-y^2}}. \quad (3.7)$$

For the new coordinates x, y on \mathbf{D}^2 we also have the constraint

$$x^2 + y^2 \leq 1. \quad (3.8)$$

Eqs.(2.49)-(2.50) take the form

$$x' = p(x, y), \quad (3.9)$$

$$y' = q(x, y), \quad (3.10)$$

where the functions p and q are given by

$$\begin{aligned} p &= \left(\sqrt{1-x^2-y^2} \left(2\sqrt{1-x^2-y^2} + y \right) - \frac{x^2}{a^2} \right) \left(\mathcal{C}_{(z,a)}(x^2-1) - x\sqrt{1-x^2-y^2} \right), \\ q &= \left(\sqrt{1-x^2-y^2} \left(2\sqrt{1-x^2-y^2} + y \right) - \frac{x^2}{a^2} \right) \left(\mathcal{C}_{(z,a)}x - \sqrt{1-x^2-y^2} \right) y \end{aligned} \quad (3.11)$$

and we redefine the derivative as follows

$$\chi' = \sqrt{1-x^2-y^2} d\chi/dA. \quad (3.12)$$

Such a redefinition of the derivative (see [38], [39]) is admissible, since, it does not change the behavior of flows, and allows us to avoid divergences, which arise for $x^2 + y^2 = 1$.

Note that the line $y = 0$ is an invariant manifold, so the flow doesn't leave it.

The critical sets of the system into the disk \mathbf{D}^2 are defined by zeroes of the RHS of eqs. (3.9)-(3.10) and include

1. the closed curve $e(a)$

$$\sqrt{1-x^2-y^2} \left(2\sqrt{1-x^2-y^2} + y \right) - \frac{x^2}{a^2} = 0, \quad (3.13)$$

2. the isolated point $p_0(z, a)$:

$$x = -\frac{\mathcal{C}_{(z,a)}}{\sqrt{\mathcal{C}_{(z,a)}^2 + 1}}, \quad y = 0. \quad (3.14)$$

Actually, there are two more points with coordinates $x = \pm 1$, $y = 0$ at which the RHS of eqs.(3.9)-(3.11) vanish. These points appear as a result of the transformation (3.7) and redefinition (3.12). They need to be taken into account to analyze the full 3d dynamical system, which we consider below.

The critical sets (3.13)-(3.14) are merely the initial critical sets (3.1)-(3.2) on \mathbf{R}^2 mapped into the disk \mathbf{D}^2 . So the closed curve $e(a)$ (3.1) comes from eq.(3.1) by gluing the infinite ends of the parabola as a result of Poincaré transformations (3.7).

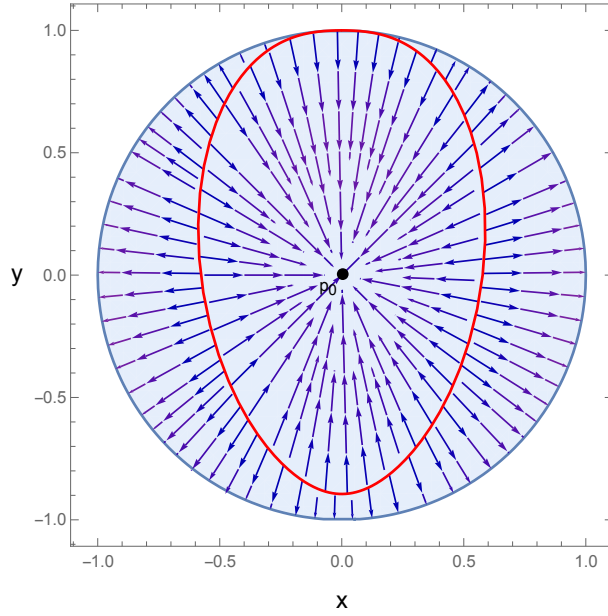


Figure 4: The flows of the system (3.9)-(3.11) with fixed z in the disk \mathbf{D}^2 . The critical curve is shown by red, while the critical point p_0 is marked by black. The parameters a^2 and z are set as: $a^2 = 0.25$ and $z = 0.5$ (so $\mathcal{C}_{(z,a)} = 0$).

| | $0 \leq z \leq z_a$ | $z_a < z < z_b$ | $z_b \leq z \leq 1$ |
|--------------------|---------------------|-----------------|---------------------|
| $0 < a^2 \leq 1/2$ | none | stable node | none |
| $a^2 > 1/2$ | unstable node | stable node | unstable node |

Table 1: The stability of the critical point p_0 for various values of a^2 and z ; z_a and z_b are values of z , at which the point p_0 intersects the critical curve $e(a)$.

Classification of stability for the critical point p_0 at various a and z is given in the Table 1. From this table we see that if $a^2 \leq \frac{1}{2}$ the point p_0 is a stable node for all z , while for $a^2 > \frac{1}{2}$ the type of stability for p_0 depends on the value of z with respect to the intersections of the critical curve $e(a)$ and p_0 . So if z lies in the region between $z = 0$ and the value of z at the first intersection of p_0 and $e(a)$ (z_a) this is an unstable node, the same is valid for z lying in the region between the value of z at the second intersection of p_0 and $e(a)$ and $z = 1$ (z_b), while if z belongs to $z \in (z_a, z_b)$, p_0 is a stable node.

It's instructive to look at the behaviour of the x -coordinate of p_0 on z . In Fig. 5 we depict the x -coordinate of p_0 on z for different a . From Fig.5 **a**) it can be seen that for $a^2 = \frac{1}{2}$ the x -coordinate as the function of z has a discontinuity in the boundary points $z = 0$ and $z = 1$. As for $a^2 > \frac{1}{2}$ we observe from Fig.5 **b**) that the x -coordinate of p_0 with $a^2 = 0.8$ vanishes for three values of z , which are related with the extrema of the scalar potential $V'_\phi = 0$, it also has two extrema, which are related with $V''_\phi = 0$. For all $a^2 > \frac{1}{2}$ the x -coordinate of p_0 has also a discontinuity at values of z , for which the scalar potential vanishes $V = 0$.

For $a^2 \leq \frac{1}{2}$ the critical point p_0 is always located inside of the critical curve. However, one should be careful with $a^2 = \frac{1}{2}$ near $z = 0$ and $z = 1$, where the point p_0 jumps due to

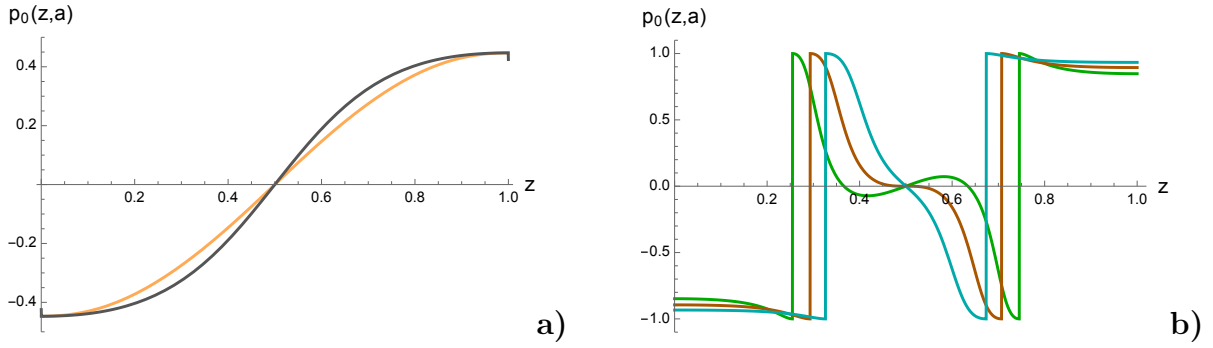


Figure 5: The dependence of the x -coordinate of p_0 on z for various a : **a)** $a^2 = 0.25$ by orange, $a^2 = 0.5$ by gray; **b)** from left to right $a^2 = 0.8$, $a^2 = 1$, $a^2 = 1.2$, correspondingly.

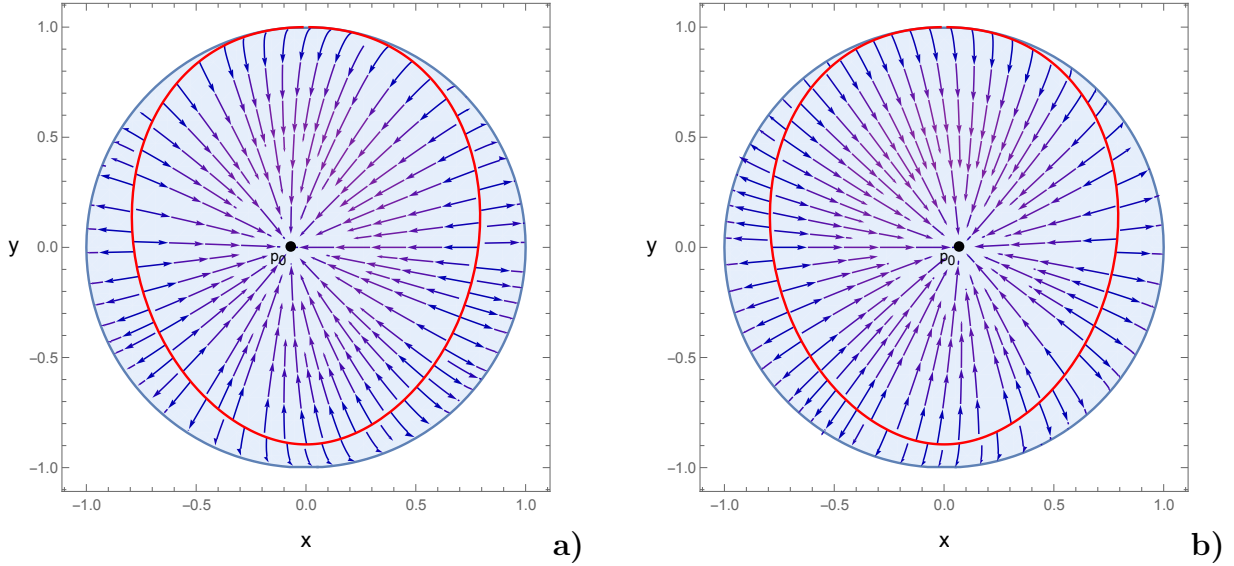


Figure 6: The flows of the system (3.9)-(3.11) with fixed z in the disk \mathbf{D}^2 : **a)** $a^2 = 0.8$, $z = 0.43$, **b)** $a^2 = 0.8$, $z = 0.58$. The critical curves are shown by red, while the critical points p_0 are marked by black.

discontinuities, see Fig. 5 **a)**. For $a^2 = 0.8$ p_0 can be both inside and outside of the critical curve. In this case, the point p_0 can also jump, that happens near regions for which $V = 0$.

In Figs. 6 the positions of p_0 and flows of the 2d system in the disk are depicted for $a^2 = 0.8$ and the values of z , which correspond to the extrema of the x -coordinate of p_0 , i.e. the values of z at which $V''_\phi = 0$.

3.2 Compactified 3d autonomous system and its critical sets

In this subsection, we discuss the 3d dynamical system in the unit cylinder and its properties.

Applying the coordinate transformations (3.7) for X and Y to eqs. (2.48)-(2.50), we

come to the dynamical system in the $3d$ unit cylinder

$$z' = z(z-1)x, \quad (3.15)$$

$$x' = p(x, y, z), \quad (3.16)$$

$$y' = q(x, y, z), \quad (3.17)$$

where p, q are given by (3.11), and we assume (3.12) for the derivatives. To describe flows of the system (3.15)-(3.17), we first discuss some of its topological properties.

The critical points and sets of eqs.(3.15)-(3.17) are:

1. xz -plane

- (a) $p_1: (0, 0, z_1); p_2: (0, 0, z_2); p_3: (0, 0, z_3)$
- (b) $p_4: (-2a^2/\sqrt{4a^4+1}, 0, 0); p_{5,6}: (\mp\sqrt{2}a/\sqrt{2a^2+1}, 0, 0)$
- (c) $p_7: (2a^2/\sqrt{4a^4+1}, 0, 1); p_{8,9}: (\mp\sqrt{2}a/\sqrt{2a^2+1}, 0, 1)$
- (d) $q_1, q_2: (-1/\sqrt{5}, 0, 0), (1/\sqrt{5}, 0, 1)$
- (e) $g_{2,3}, g_{1,4}: (\pm 1, 0, 0), (\pm 1, 0, 1)$

2. xyz -space

- (a) the closed curves $e_1, e_2: z = 0, 1; x, y \in e(a)$
- (b) the line $l: (0, 1, z), z \in [0, 1]$
- (c) the special points on line $l: \bar{p}_1, \bar{p}_{2,3} = p_1, p_{2,3} + (0, 1, 0)$
- (d) the line $\hat{l}: (0, -2/\sqrt{5}, z), z \in [0, 1]$
- (e) the special points on the line $\hat{l}: \hat{p}_1, \hat{p}_{2,3} = p_1, p_{2,3} + (0, -2/\sqrt{5}, 0)$.

The values of $z_1, z_{2,3}$ for the coordinates of the critical points $p_1, p_{2,3}, \bar{p}_1, \bar{p}_{2,3}, \hat{p}_1, \hat{p}_{2,3}$ are given by (2.46) and are related with the extrema of the scalar potential. So for $a^2 \leq \frac{1}{2}$, the points $p_{2,3}, \bar{p}_{2,3}, \hat{p}_{2,3}$ are absent. The closed curve $e(a)$ is defined by eq.(3.13). The critical points 1(a)-1(c),1(e), the critical sets 2(a)-2(e) in the unit cylinder are shown in Fig. 7 for $a^2 = 0.8$, since this case is most general. To illustrate their positions we also depict the exact half-supersymmetric RG flow from the work [33] (see Appendix A) by the orange solid curve, which connects the points p_1 and p_4 . This RG flow is plotted using x (3.7) and z (2.38) functions, which are calculated, in turn, using the scale factor A (A.1) and the scalar field ϕ (A.2).

The xz -plane is an invariant manifold of the 3d autonomous system (3.15)-(3.17). This plane is related with the zero-temperature case of holographic RG flows and was studied in the works [34, 35]. As it was mentioned above the critical points $p_{2,3}$ exist if and only if $1/2 < a^2 < 1$ (which is also true for additional 3d points $\bar{p}_{2,3}, \hat{p}_{2,3}$), since they correspond to the additional extrema of the scalar potential at $\phi_{2,3}$. The reconstruction of the metric near $p_{1,2,3}$ gives that these points correspond to AdS_3 spacetimes with different radii. We suppose that the dual field theories related to them are $\text{CFT}_1, \text{CFT}_2, \text{CFT}_3$, correspondingly.

Near points $p_4, p_{5,6}, p_7, p_{8,9}$ the gravity solutions have scaling geometries with a divergent scalar field. The dual field theories possess the scaling invariance but not the

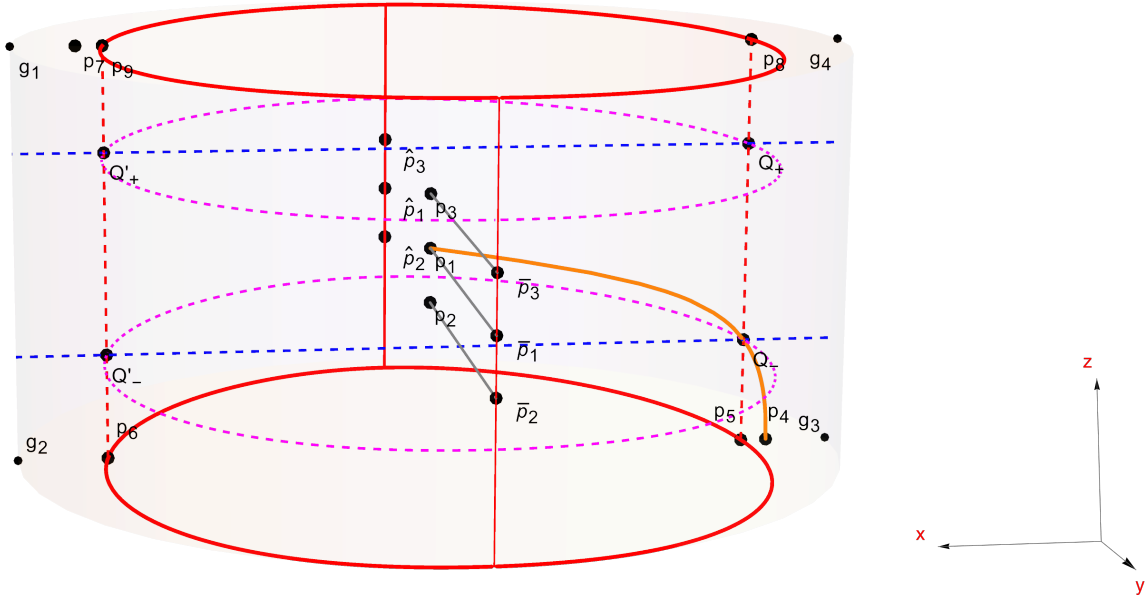


Figure 7: The location of the critical sets, regular, singular points and the exact holographic RG flow of the dynamical system (3.15)-(3.17) for $a^2 = 0.8$. The critical curves 2(a), the lines 2(b),2(d) are shown by red, the closed curves e_{\pm} by magenta (dashed), the lines N^{\pm} are shown by blue (dashed), the lines M_x^{\pm} by red (dashed). The exact holographic RG flow $p_1 - p_4$ is shown by the solid orange curve.

conformal one. In what follows we omit the discussion related to points $p_7, p_{8,9}$, since the scalar field tends to $-\infty$ for them and holographic dictionary should be completed. The exact holographic RG flow lies in the xz -plane and exists for all values of a^2 . For $0 < a^2 < \frac{1}{2}$ and $\frac{1}{2} < a^2 < 1$ it runs from p_1 (CFT₁ UV) to p_4 (IR). For the special case $a^2 = 1/2$ the points p_4, p_7 merge with p_5, p_9 , while the points q_1, q_2 , on the contrary, appear only for this case due to the behavior of $\mathcal{C}_{(z,a)}$ at $z = 0, 1$. So for $a^2 = 1/2$ the exact flow goes from p_1 (UV) to p_5 (IR) [35]. The analysis from [34, 35] shows that for the RG flows at zero temperature with the Dirichlet boundary conditions are triggered by a source of the relevant operator, CFT₁ (p_1) can be interpreted as the UV fixed point and CFT_{2,3} ($p_{2,3}$) are IR fixed points.

The classification of the critical points on the xz -plane from the point of view of the 3d system is presented in Table 2 in Appendix C.1. Note, that the points $p_{5,6}$ and $p_{8,9}$ are no longer isolated critical points in the sense of the 3d system, since they belong to the critical curves e_1 and e_2 , respectively. The points $g_{1,2,3,4}$ occur due to the Poincaré transformation (see the discussion below eqs. (3.13)-(3.14)) and were not considered in the works [34, 35]. In Appendix C.2 we briefly list possible holographic RG flows on the xz -plane with different boundary conditions.

Another invariant manifold of our 3d system (3.15)-(3.17) is given by

$$M_{xy} : (x, y) \in e(a), z \in [0, 1], \quad (3.18)$$

for which we have no dynamics on x, y .

For the case $1/2 < a^2 < 1$ the system also possess two additional sets

$$NP_{\pm} : (x, y, z_{\pm}), (x, y) \in [-1, 1], \quad (3.19)$$

where the vector field is singular, however, the points e_{\pm} arising from the intersections of M_{xy} and NP_{\pm}

$$e_{\pm} : M_{xy} \cap NP_{\pm} \quad (3.20)$$

are regular.

The presence of regular points, where the vector field seems to be singular, also occurs for the 2d dynamical system on the xz -plane, i.e. for $y = 0$. Let us illustrate what we mean by introducing the following sets

1. lines $M_x^{\pm} : (\pm\sqrt{2}a/\sqrt{2a^2+1}, 0, z), z \in [0, 1]$,
2. lines $N^{\pm} : (x, 0, z_{\pm}), x \in [-1, 1]$,
3. points $Q_{\pm}, Q'_{\pm} : Q'_{\pm} = N^{\pm} \cap M_x^+, Q_{\pm} = N^{\pm} \cap M_x^-$.

These sets are just a reduction of the sets (3.18)-(3.20) on the xz -plane. For the dynamical system on the xz -plane the lines M_x^{\pm} are invariant manifolds (there is no dynamics on x), the lines N^{\pm} are singular; but it as was noted in [35] the points Q_{\pm}, Q'_{\pm} are regular, however, the behavior of the flow near them requires some additional research.

It worth to be noted that the line l from 2(b) corresponds to the case $Y \rightarrow \infty$. Moreover, in what follows, we discuss the special points of the line l , i.e. 2(c), as near-horizon regions of black hole solutions.

We should make some comments about the points $\bar{p}_{1,2,3}$ and $\hat{p}_{1,2,3}$. We do not provide information about their stability in Table 2. Since from the point of view of the initial system (2.48)-(2.50), the points $\bar{p}_{1,2,3}$ are not critical and, generally speaking, are not strictly defined, while the points³ $\hat{p}_{1,2,3}$ lie on the critical line \hat{l} . Thus, both $\bar{p}_{1,2,3}$ and $\hat{p}_{1,2,3}$ are not isolated and not classified by standard methods through the Jacobian matrix of the linearized system. However, for the system in the cylinder (3.15)-(3.17) the points $\bar{p}_{1,2,3}$ exist, but they are not isolated. To characterize them we describe flows starting near these points, which allow us to see the difference between $\bar{p}_{1,2,3}$. Below we also conduct a brief analysis considering slices of the system (3.15)-(3.17) near these points.

3.3 Flows of the 3d autonomous system in the unit cylinder

In this subsection, we explore the behavior of the 3d system (3.15)-(3.17) in the unit cylinder for different values of the parameter a^2 . We probe the system looking numerically trajectories of eqs.(3.15)-(3.17) with certain initial conditions. In terms of coordinates in the unit cylinder (2.38),(3.7) black hole solutions near horizon correspond to points on the critical line l (see 2(b) from the list of the previous subsection), where $x = 0, y = 1, z \in [0, 1]$. The zero-temperature asymptotics correspond the xz -plane with $y = 0$. We choose the initial conditions so that the solutions start from a near-horizon region of black holes.

³In this work, we are not at all interested in the region with $Y < 0$.

3.3.1 The case $a^2 < 1/2$

Consider the case $a^2 < 1/2$, for which the scalar potential has only one extremum at $\phi = 0$ or in terms of the z -variable at z_1 . To solve eqs.(3.15)-(3.17) numerically, we impose the following initial conditions for the equations

$$x = 0, \quad y = 1 - \varepsilon, \quad z \in [z_1 - \delta, z_1 + \delta], \quad (3.21)$$

where $\varepsilon, \delta > 0$. In the initial conditions (3.21) and those we discuss below, z is actually z_h , which in turn determines the value of the scalar field at the horizon ϕ_h (2.38). These initial conditions yield two cases of trajectories, namely, the trajectories start at: 1) $z = z_1$, 2) $z < z_1$ or $z > z_1$. Numerical solutions to eqs.(3.15)-(3.17) with (3.21) for $a^2 = 0.25$ are depicted in Fig. 8. The solutions begin from the region near the line l ($x = 0, y = 1 - \varepsilon$ and ε is small), i.e. they start from the near-horizon region, then go to the xz -plane with $y = 0$, which corresponds to the zero-temperature case.

The trajectory for which $\delta = 0$ in (3.21), i.e. the initial conditions read as $(0, y - \varepsilon, z_1)$ matches with the AdS black hole solution (2.26). This trajectory is depicted by the gray line $\bar{p}_1 - p_1$ in Fig. 8 starting from the near-horizon region at \bar{p}_1 and ending at p_1 , which corresponds to the AdS asymptotics. Note, that the trajectory exists for any value of a^2 , since it is related with the extrema of the scalar potential at z_1 .

If the initial conditions are set as $(0, y - \varepsilon, z_1 \pm \delta)$, where δ is arbitrary, we obtain solutions shown by colorful curves in Fig. 8. For the trajectories with the starting points above \bar{p}_1 , we observe that they first go to the region with $x > 0$ and slowly decreasing z , then they tend to $x = 0$, while z begins to decrease faster and, finally, the trajectories end in the stable node p_1 on the xz -plane. The similar behaviour occurs for the solutions with a starting point below \bar{p}_1 with the difference, that the trajectories run into the region with $x < 0$ and slowly increasing z , which starts to increase faster tending again to the stable node p_1 at the xz -plane. It is important to notice that all such trajectories tending to p_1 pass close to the exact holographic RG flow ($p_1 - p_4$) and its mirror image (the curve $p_1 - p_7$). So the exact trajectories $p_1 - p_4$ and $p_1 - p_7$ are separatrices of the dynamical system (3.15)-(3.17). In Fig. 8 they are shown by orange curves (solid and dashed, correspondingly).

Another important feature of the system is related to the dynamics inside the invariant manifold M_{xy} (3.18), namely, all trajectories inside M_{xy} have the similar structure. To illustrate this, it is convenient to impose the following initial conditions on eqs.(3.15)-(3.17):

$$x = \rho \cos \psi, \quad y = 1 - \varepsilon, \quad z \in \rho \sin \psi + \delta, \quad (3.22)$$

with sufficiently small ρ, δ and $\psi \in [0, 2\pi]$. Then the trajectories start from a point on the circle with the center in \bar{p}_1 and the radius ρ , generally coinciding with the behaviour of the trajectories from the previous item and coming to the stable node p_1 . The solutions constructed numerically with (3.22) are shown in Fig. 9.

3.3.2 The case $1/2 < a^2 < 1$

Now we turn to the discussion of the case $1/2 < a^2 < 1$, for which the potential has three extrema at $\phi_{1,2,3}$ or in terms of z at $z_{1,2,3}$.

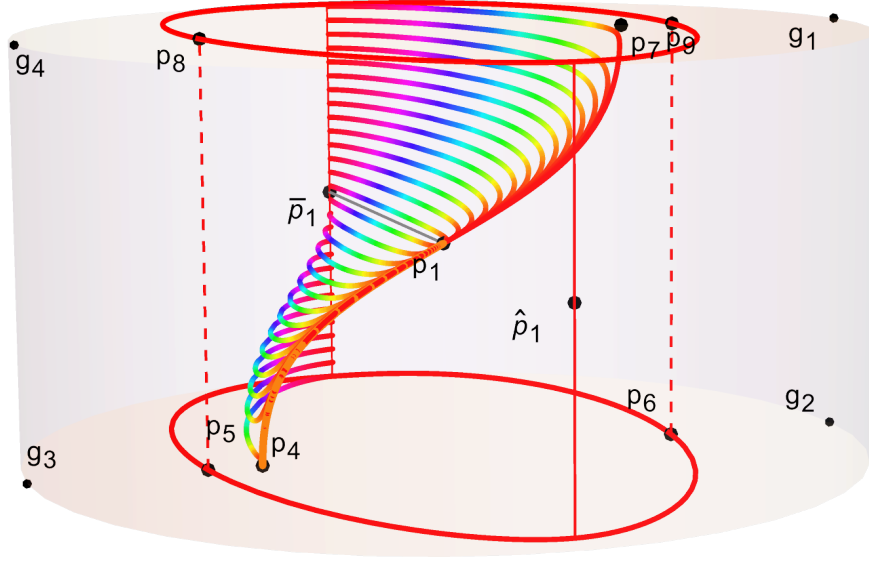


Figure 8: The trajectories of the dynamical system in the unit cylinder (3.15)-(3.17) calculated numerically for $a^2 = 0.25$ with the initial conditions (3.21) for various δ (shown by colorful curves); the AdS black hole solutions $\bar{p}_1 - p_1$ (shown by gray); the exact flows zero-temperature flows $p_1 - p_4$ and $p_1 - p_7$, which are separatrices of the system (shown by orange curves).

To find solutions of our interest to eqs. (3.15)-(3.17), which start again from the critical line l , we suppose the following class of the initial conditions:

$$x = 0, \quad y = 1 - \varepsilon, \quad z \in [z_2 - \delta, z_3 + \delta]^4, \quad (3.23)$$

where $\varepsilon, \delta > 0$ are small. These initial conditions can be naturally divided into three types:

1. $z = z_{1,2,3}$,
2. $z_2 < z < z_3$,
3. $z < z_2$ or $z > z_3$.

In Fig. 10 we depict numerical trajectories of eqs. (3.15)-(3.17) with the initial conditions (3.23) for $a^2 = 0.8$ for all cases of starting points. These solutions begin from the region near the line l , with $y = 1 - \varepsilon$, and, then, tend to the xz -plane with $y = 0$, i.e. to the zero-temperature plane, however, otherwise they behave differently. Below we give the classification of these flows in details.

1. Fixing the initial conditions for the system as: $(0, y - \varepsilon, z_{1,2,3})$, i.e. $\delta = 0$, we obtain three solutions coinciding with the exact AdS black holes (2.26) (see also Appendix B). From the point of view of the phase diagram the trajectories are lines, that connect the points $\bar{p}_{1,2,3}$ with the points $p_{1,2,3}$, respectively. We show the trajectories $\bar{p}_{1,2,3} - p_{1,2,3}$

⁴We recall that the points z corresponding to the extrema of the scalar potential have the following order $z_2 < z_1 < z_3$.

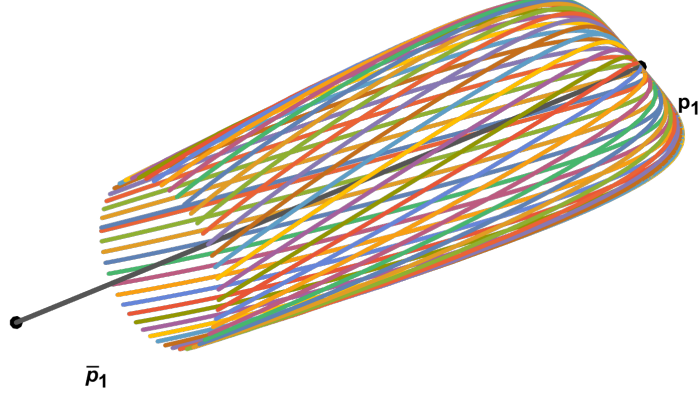


Figure 9: The numerical trajectories of the dynamical system (3.15)-(3.17) for $a^2 = 0.25$ with the initial conditions (3.22) inside the invariant manifold M_{xy} (3.18). For the initial conditions we fix $\rho = 0.1$, $\delta = 0.5$ and $\varepsilon = 0.2$. The exact AdS black hole solution $\bar{p}_1 - p_1$ is shown by gray.

by gray color in Fig. 10. Note, that we have three different AdS black hole solutions corresponding to the extrema of the potential. Moreover, types of stability of the ending points $p_{1,2,3}$ are different, see Table 2. So the solution $\bar{p}_1 - p_1$ is related with the thermal state of UV CFT₁, while $\bar{p}_2 - p_2$ and $\bar{p}_3 - p_3$ are related with the thermal states of IR CFT₂ and CFT₃, respectively.

2. (a) Let us fix the initial conditions as: $(0, y - \varepsilon, z_1 \pm \delta)$, where δ is not necessarily small, so, that the starting point on the z axis should not be below z_2 or above z_3 . These solutions are shown by olive in Fig. 10. Note, that if we take $\delta \rightarrow 0$, then such a solution is almost identical to the solution $\bar{p}_1 - p_1$ from item 1. The trajectories behave as follows. Setting the initial point along the z -axis below the point \bar{p}_1 , the trajectory first tends to the region with a negative x , while z slowly increases, then, the trajectory runs to $x = 0$, and z increases faster, i.e. the closer the solutions are to the xz -plane, the faster z grows, and eventually the trajectory ends at the stable node p_1 . One can give a similar description for a trajectory that begins above \bar{p}_1 . The difference is that this trajectory tends to the region with positive x , while z slowly decreases, then, the solution goes to $x = 0$, and z decreases faster, so the solution reaches the stable critical point p_1 .
- (b) Now we set the initial conditions as: $(0, y - \varepsilon, z_{2,3} \pm \delta)$. As a result, we get two trajectories, which connect $\bar{p}_{2,3}$ and p_1 passing the unstable (saddles) critical points $p_{2,3}$ with $y = 0$. We depict these flows by dark blue color in Fig. 10. In this case there is some peculiarity, namely, if one sends $\delta \rightarrow 0$, the flow can be conditionally split into two parts, i.e. $\bar{p}_{2,3} - p_{2,3}$ and $p_{2,3} - p_1$. Moreover, the smaller δ , the closer the first part of the flow is to the exact AdS black hole solution (connecting $\bar{p}_{2,3}$ and $p_{2,3}$), which was described above; and the second

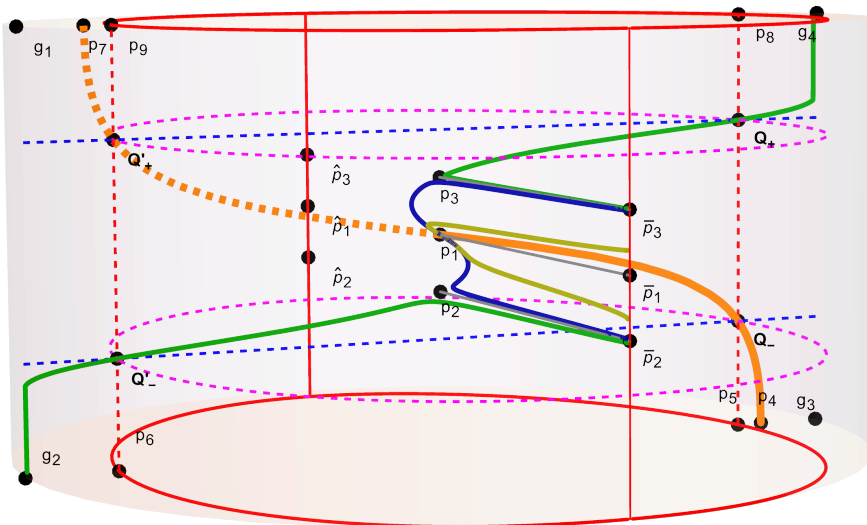


Figure 10: Numerical solutions, exact solutions, critical sets, regular and singular points of the 3D dynamical system (3.15)-(3.17) with $a^2 = 0.8$ in the unit cylinder. Numerical trajectories on the figure are: $\bar{p}_{1,2,3} - p_{1,2,3}$ (shown by gray), $\bar{p}_{2,3} - p_1$ (shown by blue), $\bar{p}_2 - g_2$, $\bar{p}_3 - g_4$ (both shown by green), numerical solutions from 2(b) of (both shown by olive). The exact solutions $p_1 - p_4$ and its mirror image $p_1 - p_7$ are shown by thick orange curves (solid and dashed, correspondingly).

part is closer to the flow between two pure AdS solutions with different radii, $p_{2,3} - p_1$, which have been considered in the works [34, 35].

3. Fixing the initial conditions as: $(0, y - \varepsilon, z_{2,3} \mp \delta)$ with small δ , we find the solutions from $\bar{p}_{2,3}$ to the stable critical points $g_{2,3}$. These solutions can be interpreted as naked singularities. We depict the trajectories by green color in Fig. 10. Let us discuss a solution, which starts at $(0, y - \varepsilon, z_2 - \delta)$ (a similar description can be given for the second flow, which starts near z_3). For small δ , the solution is splitted into two parts: $\bar{p}_2 - p_2$ and $p_2 - g_2$. Again, the smaller δ , the more the first part coincides with the AdS black hole solution ($\bar{p}_2 - p_2$), described above in the first item. The part of the solution $p_2 - g_2$ lies in the invariant xz -plane, passing through the regular point Q'_- . It worth to be noted, that the points $g_{2,3}$ correspond to scaling singular geometries, which do not satisfy Gubser's bound, so these flows are not well defined from the point of view of holography.

The behavior of the solutions with the initial conditions (3.23) imposed is always exactly the same as we presented above. This can be understood from the following observation: we determine the dynamics of the trajectory in the xy -plane using by the position of the critical point p_0 with the coordinates given by (3.14), which in turn depend on z . Then the dynamics along the z -axis is determined directly from the simple equation (3.15) and mostly depends on a sign of x . We should also take into account that the motion in the xy -plane affects the motion along the z -axis and vice versa.

Consider the trajectory from item 2(b). For the initial condition (3.23), we choose the value of z such that $z_2 < z < z_1$ and $z < (z_1 - z_2)/2$, i.e. it lies closer to z_2 than to z_1 . The

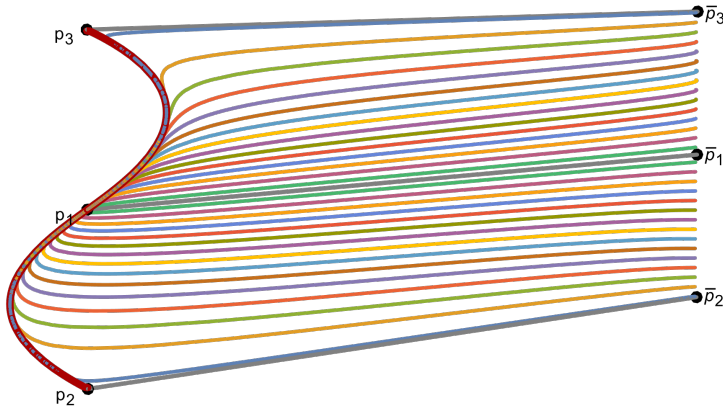


Figure 11: The numerical trajectories of the dynamical system (3.15)-(3.17) for $a^2 = 0.8$ with the initial conditions (3.23) and the separatrices $p_1 - p_2$, $p_2 - p_3$.

solution runs from the region below the point \bar{p}_1 with slowly increasing z . To understand the dynamics of the trajectory in the xy -plane, we need to take a look at Section 3.1. The point p_0 in this case is a stable node (see Table 1), which is located in the negative region of x (see the green curve in Fig. 5 **b**). Therefore, the flow tends to p_0 , decreasing in both x and y . As far as $x < 0$, z grows, that follows from eq. (3.15). Next, since z increases, then from Fig. 5 **b**) it follows that the position of the point p_0 goes further and further into the negative region of x until z passes the local minimum of the function $p_0(z, a)$, which is located between z_2 and z_1 and corresponds to $V''_\phi = 0$ (see Fig. 5 **b**) again). After passing this minimum, the position of p_0 along x tends to $x = 0$, but at the same time, since x is still negative, z grows. Finally, the trajectory ends at the stable node p_1 with $x = 0$.

It is important to note that black hole solutions with the initial conditions (3.23) such that $z_2 < z < z_1$ or $z_1 < z < z_3$, i.e. the values of the scalar field on the horizon ϕ_h takes a value between extrema of the scalar potential, pass close to the trajectories $p_1 - p_2$ and $p_1 - p_3$, which are holographic RG flows between two AdS fixed points [35]. Thus, the flows $p_1 - p_2$ and $p_1 - p_3$ are separatrices in this case. We depict these solutions in Fig.11.

One can consider a more general class of initial conditions comparing to (3.23)⁵, namely

$$x = 0 \pm v, \quad y = 1 - \varepsilon, \quad z \in [z_2 - \delta, z_3 + \delta], \quad (3.24)$$

i.e. we add a variation by x with small $\varepsilon, v > 0$ such that v and ε respect the constraint (3.8). Thus, the initial conditions are splitted into the following cases:

1. $x = \pm v, \quad y = 1 - \varepsilon, \quad z = z_{1,2,3}$.

- (a) For the initial conditions $(-v, y - \varepsilon, z_1)$ the solution starts from the region near \bar{p}_1 with negative x . First, y decreases and z increases (see eq. 3.15), such that in the xy -plane the flow tends to the attracting point p_0 (a stable node, see Table 1). The coordinate x starts to increase being negative, so p_0 tends into the region with $x > 0$, see Fig. 4 and Figs. 6 **a**) and **b**). Since x is still negative, z increases but more and more slowly. Next, x reaches 0, p_0 turns and goes to

⁵For the readability we have split the discussion of the initial conditions (3.23) and (3.24)

the direction, where $x < 0$, while z starts to decrease. So the trajectory ends at the stable p_1 .

- (b) The trajectory with the initial conditions $x = v$, $y = 1 - \varepsilon$, $z = z_1$ begins near \bar{p}_1 with positive x . Here, since $x > 0$, z decreases as well as y and the trajectory tends again to the stable node p_0 in the xy -plane. The point p_0 goes to the region with $x < 0$. The coordinate z decreases slowly, and begins to increase when x reaches 0. Finally, the trajectory ends at p_1 .
- (c) Imposing the initial conditions $x = 0 - v$, $y = 1 - \varepsilon$, $z = z_2$ and $x = 0 + v$, $y = 1 - \varepsilon$, $z = z_3$ on eqs. (3.15)-(3.17) gives rise the trajectories, which are similar to $\bar{p}_2 - p_2 - p_1$ and $\bar{p}_3 - p_3 - p_1$, correspondingly. This behaviour was described in item 2(a) of the previous list.
- (d) Changing the sing of v in the conditions from the previous item yields the trajectories that start from $\bar{p}_{2,3}$, then pass through Q'_- and Q_+ , respectively and go $z = 0, 1$, that correspond to $\phi \rightarrow \pm\infty$.

Note, that the flows with the initial conditions (3.23) considered above behave monotonically on z , while for the trajectories with the initial conditions $x = 0 \pm v$, $y = 1 - \varepsilon$, $z = z_1$ the behaviour on z is non-monotonic.

2. The flows with the initial conditions $x = 0 \pm v$, $y = 1 - \varepsilon$, $z = z_1 \pm \delta$ can have both monotonic and non-monotonic behaviours with respect to z , but finally end in the same stable point p_1 . For them, a picture similar to Fig. 9 is valid. In the next section we will present analytical formulas to describe these trajectories near the point \bar{p}_1 .
3. Assuming the initial conditions of the type: $x = \pm v$, $y = 1 - \varepsilon$, $z = z_{2,3} \pm \delta$, we construct the flows, which do not necessarily end in the stable critical point p_1 , in contrast to the trajectories from the previous item. To illustrate the most significant feature of such flows, let us describe a trajectory starting near the fixed point \bar{p}_3 (the case of the flows from \bar{p}_2 can be described similarly). Consider, for example, the initial condition of the form $(-v, e - \varepsilon, z_3 - \delta)$. First, recall that if $v = 0$ we would get a flow from \bar{p}_3 running to the point p_1 passing p_3 (see Fig. 10). However, a suitable variation of the initial conditions along x in the negative direction can lead to a flow going directly to the stable point g_4 passing the unstable point p_3 , see Table 2. A similar picture is observed for the initial conditions $x = v$, $y = e - \varepsilon$, $z = z_3 + \delta$. In this case, with a certain choice of v , the flow can go to p_1 , however as it has already been described above (see Fig. 10), for $v = 0$ the flow definitely goes to g_4 .

In fact, the behavior of the trajectories specified by the initial conditions (3.24) can be described as follows. Let us consider the motion of a point one-dimensional particle in the potential with a minimum at the origin and two symmetric maxima to the left and right of the origin, that is, the potential of a type, which is inverse to the potential shown in Fig. 1 with $a^2 = 0.8$. Let the coordinate of the point be denoted as $x(A)$, and the velocity as $\dot{x}(A)$, where A is time. It is not difficult to verify that the functions $z(A)$ and $-x(A)$ in the cylinder behave like the quantities $x(A)$ and $\dot{x}(A)$, respectively. In Fig.12 we show the

possible dynamics of the particle. In Fig.12 a) we depict the trajectory of the point particle, which begins at the point \bar{p}_3 with the velocity $-\dot{x}(A) = v$ such that $v > 0$ and ends at the minimum p_1 . This trajectory corresponds to the flow from the list 1(c) with (3.24). In Fig. 12 b) we show the case, when the particle starts its motion from $\bar{p}_3 + \delta$ towards p_3 with a quite small velocity $-\dot{x}(A) = v$, $v > 0$. Before reaching the point p_3 , the particle changes the direction of motion and ends the trajectory at the point g_4 .

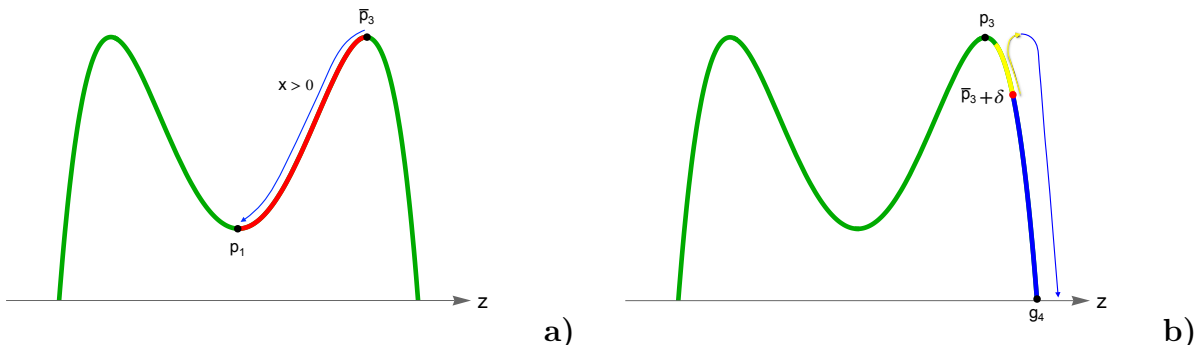


Figure 12: The motion of the point particle with different initial conditions. a) The trajectory begins at the point \bar{p}_3 with $x = v$, such $v > 0$, and ends at the point p_1 . The red stripe in the figure shows the trajectory of the particle, the blue arrow indicates the direction of motion. b) The trajectory begins at $\bar{p}_3 + \delta$, with $x = v$ where $v > 0$ is sufficiently small. The trajectory first moves towards the point p_3 , this part of the trajectory is depicted by yellow, while the direction of motion is marked by the yellow arrow. At certain moment, x becomes negative and $\dot{z} > 0$. As a result, the trajectory moves to g_4 , this part of the trajectory is shown by blue, the direction of motion is shown by the blue arrow.

In the next section we will obtain analytical formulas for the flows near the critical line l described above.

4 Near-horizon solutions from the dynamical system

In this section, we reconstruct asymptotic finite temperature solutions near the fixed points. The solutions can be associated with near-horizon geometries of asymptotically AdS black holes. We also briefly discuss properties of the fixed points on the line l .

4.1 Qualitative analysis of critical points at finite temperature

In this subsection we give a qualitative analysis of fixed points of the $3d$ system (3.15)-(3.17) in the cylinder, which are related with non-zero temperature. Let us consider a region of our $3d$ system (3.15)-(3.17) near the critical line l , i.e. under the condition $x \sim 0$ and $y \sim 1$. It is convenient to rewrite the latter condition introducing a new variable ζ , so that

$$y = 1 - \zeta, \tag{4.1}$$

with a sufficiently small ζ . Taking into account (4.1) and keeping only the first order in x and ζ we represent

$$\sqrt{1 - x^2 - y^2} \sim \sqrt{2\zeta}. \quad (4.2)$$

Plugging (4.1) and (4.2) into eqs. (3.15)-(3.17) and keeping the most significant contributions in x and ζ , we are brought to the following dynamical system

$$\frac{dz}{dA} = \frac{z(z-1)x}{\sqrt{2\zeta}}, \quad (4.3)$$

$$\frac{dx}{dA} = -\mathcal{C}_{(z,a)}, \quad (4.4)$$

$$\frac{d\zeta}{dA} = \sqrt{2\zeta}, \quad (4.5)$$

where it is convenient to come from the derivatives defined by eq. (3.12) to ordinary ones.

Before solving eqs. (4.3)-(4.5), we will discuss some interesting properties of trajectories of the 2d dynamical system, which is obtained as a slice of the system (4.3)-(4.5) along the variable ζ ($0 < \zeta \ll 1$). Fixing ζ the system (4.3)-(4.5) reduces to

$$z' = z(z-1)x, \quad (4.6)$$

$$x' = -\mathcal{C}_{(z,a)}\sqrt{2\zeta}, \quad (4.7)$$

where we again use the redefinition of the derivatives (3.12) taking into account (4.2) to eliminate the divergence at $\zeta \rightarrow 0$. The dynamical system (4.6)-(4.7) on the xz -plane at some $\zeta \neq 0$ has the following critical points

$$\mathbf{z}_1 = (z_1, 0), \quad \mathbf{z}_2 = (z_2, 0), \quad \mathbf{z}_3 = (z_3, 0), \quad (4.8)$$

with the z -coordinates corresponding to the extrema of the potential (2.46). Thus, for $0 < a^2 \leq \frac{1}{2}$ we have only one critical point z_1 , since z_2, z_3 turn to be complex in this case, while for $\frac{1}{2} < a^2 < 1$ there are three critical points. The critical points can be considered as a projection of the critical points $\bar{p}_{1,2,3}$ onto the xz -plane with a non-zero y , which is close 1.

To classify the points \mathbf{z}_i we find the eigenvalues λ_1^i, λ_2^i of the Jacobian matrix of the linearized system (4.6)-(4.7). Omitting the calculations we get

$$\lambda_{1,2}^i = \pm(2\zeta)^{1/4} \left(\sqrt{|z(z-1)|} \sqrt{\frac{d\mathcal{C}_{(z,a)}}{dz}} \right) \Big|_{z=z_i}, \quad (4.9)$$

where $i = 1, 2, 3$.

Below we consider the case $\frac{1}{2} < a^2 < 1$, then the following expressions are valid

$$\frac{d\mathcal{C}_{(z,a)}}{dz} \Big|_{z=z_1} < 0, \quad \frac{d\mathcal{C}_{(z,a)}}{dz} \Big|_{z=z_{2,3}} > 0. \quad (4.10)$$

Thus, if $\zeta \neq 0$ the point \mathbf{z}_1 is center and the points $\mathbf{z}_{2,3}$ are saddles. The phase portraits of the system (4.6)-(4.7) with $a^2 = 0.8$ are shown in Fig.13a) and b) for $\zeta = 0$ and $0 < \zeta \ll 1$, correspondingly.

The value ζ in (4.6)-(4.7) can be considered as a bifurcation parameter of the dynamical system: at $\zeta = 0$, phase portraits in small neighborhoods of points z_i look the same (see Fig. 13 **a**)), and as ζ increases, a center is formed near z_1 , and saddles are formed near $z_{2,3}$ (see Fig. 13 **b**)).

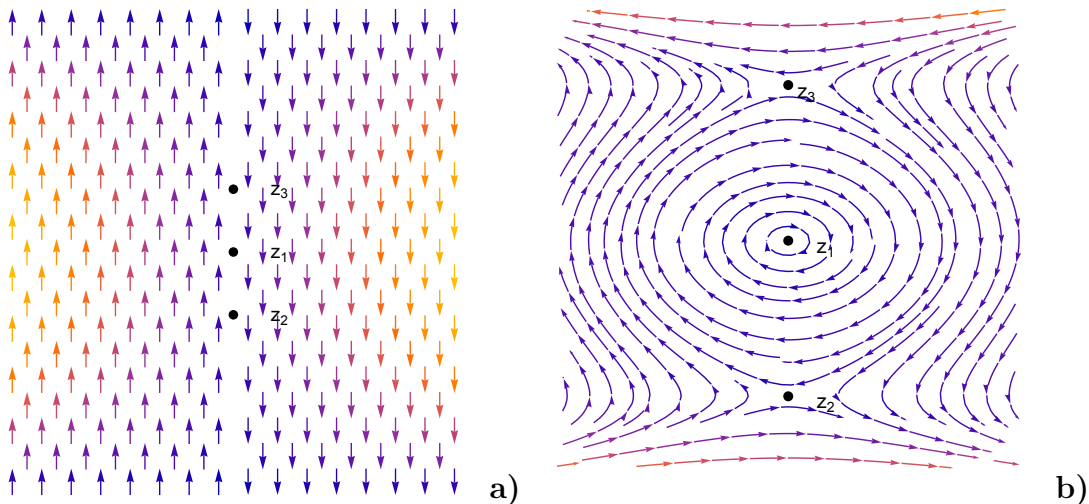


Figure 13: Phase portrait of the system (4.6)-(4.7) in small neighborhoods of the points z_i for $a^2 = 0.8$: **a)** $\zeta = 0$, **b)** $0 < \zeta \ll 1$.

This estimation of stability for the critical points $\bar{p}_{1,2,3}$ allows to assume that the critical point \bar{p}_1 is stable, while $\bar{p}_{2,3}$ are unstable. However, we note this estimation should be improved, for instance, by the center manifold analysis [44] as it was done in [41].

4.2 Reconstruction of asymptotic solutions near critical points

In this subsection we derive solutions for the metric functions A , f and the scalar field ϕ near fixed points at finite temperature, i.e. we construct near-horizon AdS black-hole solutions.

Below we show that near the critical points $\bar{p}_{1,2,3}$ (and in general near the critical line l on which these points lie, see Fig. 7) a simplified version of the system (4.3)-(4.5) can be solved exactly. Solutions of this simplified system fully reproduce the flows near the l line described in the previous section (see Fig. 6 or Fig. 10). However to restore the metric functions A and f we will use the simplest class of these solutions.

As one can see, the latter equation of the system (4.3)-(4.5) is independent of other variables and can be solved immediately

$$\zeta = \frac{1}{2}(A - A_h)^2, \quad (4.11)$$

where A_h is some positive constant (see Appendix B). Taking into account (4.11), we can

rewrite the remaining two equations of (4.3)-(4.4) in the following form

$$\frac{dz}{dA} = \frac{z(z-1)x}{(A-A_h)}, \quad (4.12)$$

$$\frac{dx}{dA} = -\mathcal{C}_{(z,a)}. \quad (4.13)$$

In terms of the original variables X and Y (see eqs.(2.48)-(2.50)), the system (4.12)-(4.13) is represented as

$$\frac{dz}{dA} = z(z-1)X, \quad (4.14)$$

$$\frac{dX}{dA} = -\frac{1}{(A-A_h)}(X + \mathcal{C}_{(z,a)}), \quad (4.15)$$

where the coordinate transformations (3.7), are used. This is in agreement with the equations for X and Y near horizon from [24].

Note, that eqs. (4.14)-(4.15) can be obtained from the original equations (2.48)-(2.50) almost immediately if we send $Y \rightarrow \infty$ for them. In this case, the equation in Y is also separated and has a solution

$$Y(A) = \frac{1}{A-A_h}. \quad (4.16)$$

Plugging eq. (4.16) back into the remaining ones (2.48)-(2.50), we get exactly eqs. (4.14)-(4.15).

To rewrite eqs. (4.14)-(4.15) in a simpler form, it is convenient to come from the variable z back to ϕ , i.e. to use the transformation (2.38). Then the system (4.14)-(4.15) reads as

$$\frac{d\phi}{dA} = X, \quad (4.17)$$

$$\frac{dX}{dA} = -\frac{1}{(A-A_h)} \left(X + \frac{a^2 V_\phi(\phi)}{2 V(\phi)} \right), \quad (4.18)$$

where the definition of $\mathcal{C}_{(\phi,a)}$ (2.44) is used. Eqs. (4.17)-(4.18) are easily reduced to a single second order equation

$$(A-A_h) \frac{d^2\phi}{dA^2} + \frac{d\phi}{dA} + \frac{a^2 V_\phi(\phi)}{2 V(\phi)} = 0. \quad (4.19)$$

Next, we want to consider a simplification of this equation. For this we expand the last term in a Taylor series up to the first order near one of the extrema $\phi_h = \phi_{1,2,3}$ of the potential. As a result we obtain

$$(A-A_h) \frac{d^2\phi}{dA^2} + \frac{d\phi}{dA} + \frac{a^2 V_{\phi\phi}(\phi_h)}{2 V(\phi_h)} (\phi - \phi_h) = 0, \quad (4.20)$$

where we used that ϕ_h is also a critical point of the potential, i.e. $V_\phi(\phi_h) = 0$.

We are looking for solutions to the latter equation with the following initial conditions

$$\phi(\varepsilon) = \phi_h + \delta, \quad \phi'(\varepsilon) = v, \quad (4.21)$$

where ε, δ, v are small, $\varepsilon > 0$ and δ, v may have an arbitrary sign. The choice of the initial conditions (4.21) means that solutions of our interest are those near the critical points $\bar{p}_{1,2,3}$ in the cylinder, see Fig. 10. It worth to be noted that we assume $\varepsilon^2 = \delta^2 = 0$, but v^2 may not be zero⁶.

Solving eq.(4.20) we also must take into account the sign of the coefficient in front of $\phi(A)$, i.e.

$$\Delta_i^{(h)} := \frac{a^2 V_{\phi\phi}(\phi_h)}{2 V(\phi_h)}, \quad (4.22)$$

with $i = 1, 2, 3$. It is interesting to note that the components of the eigenvalues of the critical points (4.8) have the same structure (4.10) as (4.22). At the same time one can recognise in (4.22) a combination of the conformal dimension (2.30) and the radius of an AdS spacetime ℓ . Assuming that $\frac{1}{2} < a^2 < 1$, as a more general case, we get the conditions

$$\Delta_1^{(h)} = -2a^2(a^2 - 1) > 0, \quad \Delta_{2,3}^{(h)} = 4(a^2 - 1) < 0. \quad (4.23)$$

Note, that for the case $0 < a^2 \leq \frac{1}{2}$, the relation for $\Delta_1^{(h)}$ (4.23) holds.

Let us first consider the case $\phi_h = \phi_1$, i.e. the value of the scalar field on the horizon is the same as at the extremum of the potential related with CFT_1 UV. Taking into account (4.23) the general solution to the scalar field equation (4.20) can be written in the form

$$\phi(A) = \phi_1 + c_1 J_0 \left(2\sqrt{\Delta_1^{(h)}(A - A_h)} \right) + c_2 Y_0 \left(2\sqrt{\Delta_1^{(h)}(A - A_h)} \right), \quad (4.24)$$

where J_0 and Y_0 are the Bessel functions of the first and second kinds, correspondingly. Expanding in series (4.24) by A near A_h up to the first order we obtain

$$\phi(A) = \phi_1 + (1 - A)c_1 + \frac{c_2}{\pi} \left(2\gamma + \ln A - A(2(\gamma - 1) + \ln A) \right), \quad (4.25)$$

where γ is Euler–Mascheroni constant and for convenience we introduce $A := \Delta_1^{(h)}(A - A_h)$. Then the constants c_1 and c_2 are

$$c_1 = \delta + \left(\Delta_1^{(h)} \delta (1 - \ln(\Delta_1^{(h)} \varepsilon) - 2\gamma) - v(\ln(\Delta_1^{(h)} \varepsilon) + 2\gamma) \right) \varepsilon, \quad (4.26)$$

$$c_2 = \pi \varepsilon (\Delta_1^{(h)} \delta + v). \quad (4.27)$$

Now we proceed with the reconstruction of the metric functions $A(w)$ and $g(w)$. By virtue of eqs. (2.37) and (4.16) the function $f(A)$ has the form

$$f(A) \simeq e^{c_g} (A - A_h). \quad (4.28)$$

that is the same as for the reconstructed AdS black hole solution from the reduced dynamical system with the constant scalar field, see Appendix B.2.

To find A we subtract eq. (2.23) from (2.21), that brings us to the following equation

$$\ddot{A} + \frac{\dot{\phi}^2}{a^2} = 0. \quad (4.29)$$

⁶In fact, we have already significantly used the first two relations in the derivation of eq. (4.20)

Using the solution (4.25) with (4.26)-(4.27) and assuming $\varepsilon \sim 0$, we obtain the following equation for the scalar factor A

$$\ddot{A} = 0. \quad (4.30)$$

From the latter we find that the solution for A near the horizon reads

$$A \simeq \sqrt{-\frac{V(\phi_h)}{2}} w, \quad (4.31)$$

where the constants of integration are found as in Appendix B.2 and $\phi_h = \phi_1$. Owing to (4.28),(4.31) and choosing $c_g = \ln 2$ (see Appendix B.2), the near-horizon metric takes the form

$$ds^2 \simeq e^{2\sqrt{-\frac{V(\phi_h)}{2}}w} \left(-\sqrt{-2V(\phi_h)}(w - w_h)dt^2 + dx^2 \right) + \frac{dw^2}{\sqrt{-2V(\phi_h)}(w - w_h)}. \quad (4.32)$$

Note, that the assumption $\varepsilon \sim 0$ leads to the special solution with $c_2 = 0$ and the second initial condition (4.21) turns to be

$$\phi'(0) = -\delta\Delta_1^{(h)}, \quad (4.33)$$

where $\Delta_1^{(h)}$ defined by (4.23). This yields that the solution to (4.25) for the scalar field is a linear function

$$\phi \simeq \left(1 - \Delta_1^{(h)} \sqrt{-\frac{V(\phi_h)}{2}}(w - w_h) \right) \delta. \quad (4.34)$$

We see that the near-horizon form of the scale factor A (4.31) and blackening function f (4.28) are the same as those for a near-horizon AdS black hole solution found in Appendix B.2. The scalar field (4.34) vanishes as we send δ to zero $\delta \rightarrow 0$.

In the same way we are able to find similar representation for the metric functions and scalar field for the case when the value of the scalar field on the horizon is as at the other critical points of the potential, $\phi_h = \phi_{2,3}$.

4.3 Generalization for an arbitrary ϕ_h

In this subsection we obtain a near-horizon dilatonic black hole solution for our model when the value of the scalar field at the horizon ϕ_h is not necessarily the value at the critical point of $V(\phi)$.

Expansion in series of the last term of the scalar field equation (4.19) near an arbitrary ϕ_h yields to

$$\frac{a^2 V_\phi(\phi)}{2 V(\phi)} \Big|_{\phi_h} \cong \frac{a^2}{2} \left(\frac{V_\phi(\phi_h)}{V(\phi_h)} + \left(\frac{V_{\phi\phi}(\phi_h)}{V(\phi_h)} - \frac{V_\phi(\phi_h)^2}{V(\phi_h)^2} \right) (\phi - \phi_h) \right), \quad (4.35)$$

$$= \Lambda^{(h)} + \left(\Delta^{(h)} - \frac{2}{a^2} (\Lambda^{(h)})^2 \right) (\phi - \phi_h), \quad (4.36)$$

$$= \Lambda^{(h)} + \mathbf{K}^{(h)} (\phi - \phi_h), \quad (4.37)$$

where we denote

$$\Lambda^{(h)} = \frac{a^2 V_\phi(\phi_h)}{2 V(\phi_h)}, \quad \Delta^{(h)} = \frac{a^2 V_{\phi\phi}(\phi_h)}{2 V(\phi_h)}, \quad \mathbf{K}^{(h)} = \left(\Delta^{(h)} - \frac{2}{a^2} (\Lambda^{(h)})^2 \right). \quad (4.38)$$

Note, that for $a^2 \leq \frac{1}{2}$ the quantity $\mathbf{K}^{(h)}$ is always non-negative, while for $\frac{1}{2} < a^2 < 1$ we have to trace the sign of $\mathbf{K}^{(h)}$ with respect to the position of ϕ_h and also take into account zeros of the scalar potential.

The solution to eq. (4.20) can be represented as follows

$$\phi(A) = \begin{cases} c_1 J_0 \left(2\sqrt{\mathbf{K}^{(h)}(A - A_h)} \right) + c_2 Y_0 \left(2\sqrt{\mathbf{K}^{(h)}(A - A_h)} \right) + \phi_h - \frac{\Lambda^{(h)}}{\mathbf{K}^{(h)}}, & \text{for } \mathbf{K}^{(h)} > 0, \\ c_1 I_0 \left(2\sqrt{|\mathbf{K}^{(h)}(A - A_h)|} \right) + c_2 K_0 \left(2\sqrt{|\mathbf{K}^{(h)}(A - A_h)|} \right) + \phi_h - \frac{\Lambda^{(h)}}{\mathbf{K}^{(h)}}, & \text{for } \mathbf{K}^{(h)} < 0, \end{cases} \quad (4.39)$$

where I_0 and K_0 are modified Bessel functions of the first and second kinds, correspondingly. The expansion in series of the scalar field (4.39) near A_h up to the first order regardless of the sign of $\mathbf{K}^{(h)}$ can be represented in the form

$$\phi(\bar{A}) = \phi_h - \frac{\Lambda^{(h)}}{\mathbf{K}^{(h)}} + \tilde{c}_1(1 - \bar{A}) + \tilde{c}_2(2\gamma + \ln|\bar{A}| - \bar{A}(2(\gamma - 1) + \ln|\bar{A}|)), \quad (4.40)$$

where $\bar{A} = \mathbf{K}^{(h)}(A - A_h)$ and the constants of integration \tilde{c}_1, \tilde{c}_2 are chosen in the form

$$\tilde{c}_1 = \frac{\Lambda^{(h)}}{\mathbf{K}^{(h)}} + \varepsilon(\Lambda^{(h)} - 2\gamma(\Lambda^{(h)} + v) - (\Lambda^{(h)} + v) \ln(|\mathbf{K}^{(h)}\varepsilon|)), \quad \tilde{c}_2 = \varepsilon(\Lambda^{(h)} + v). \quad (4.41)$$

To find the scale factor A we use the equation (4.29) rewritten in the following form

$$\ddot{A} + \dot{A}^2 \left(\frac{d\phi(A)}{dA} \right)^2 = 0. \quad (4.42)$$

Plugging into eq.(4.42) only the leading term of the quantity $\left(\frac{d\phi}{dA} \right)^2$ with $\varepsilon = 0$, we find that eq.(4.42) reduces to

$$\ddot{A} + \frac{\Lambda^{(h)}}{a^2} \dot{A}^2 = 0. \quad (4.43)$$

Then, the solution for A reads

$$A(w) = \frac{a^2}{(\Lambda^{(h)})^2} \ln \left(\frac{(\Lambda^{(h)})^2}{a^2} w + C_1 \right) + C_2, \quad (4.44)$$

where C_1 and C_2 are constants of integration, which will be determined below from fairly simple considerations. The solution for $A(w)$ (4.44) should reproduce the near-horizon AdS black hole solution (2.26) if ϕ_h is the critical point of the potential. Remembering that for such points of the potential $\Lambda^{(h)} = 0$, since $V'(\phi_h) = 0$, we expand in series the scale factor (4.44) assuming that the parameter $\Lambda^{(h)}$ is small, as a result we obtain

$$A(w) \simeq C_2 + \frac{\ln(C_1)a^2}{(\Lambda^{(h)})^2} + \frac{w}{C_1} + o((\Lambda^{(h)})^2). \quad (4.45)$$

Thus, choosing the integration constants C_1 and C_2 in the following form

$$C_2 = -\frac{\ln(C_1)a^2}{(\Lambda^{(h)})^2}, \quad C_1 = \sqrt{-\frac{2}{V(\phi_h)}}, \quad (4.46)$$

and substituting them into eq.(4.45), we automatically recover the scale factor of the near-horizon AdS solution (2.26). Owing to C_2 (4.46) from (4.44) we obtain

$$A(w) = \frac{a^2}{(\Lambda^{(h)})^2} \ln \left(\frac{\frac{(\Lambda^{(h)})^2}{a^2}w + c_A}{c_A} \right), \quad (4.47)$$

where we redefine C_1 as c_A for convenience.

Now we are able to restore the blackening function f near the horizon. By virtue of (4.16) and the definition of Y (2.37), the function $g(A)$ reads

$$g(A) = c_g + \ln(A - A_h). \quad (4.48)$$

Note, that g given by (4.48) matches with g for the exact AdS black hole (B.19) in terms of A , however, the constants c_g in (4.48) and (B.19) are different. We find c_g in (4.48) as it was done for the AdS black hole in Appendix B.2. Using the definition of Y (2.37) we find that eq.(2.21) near horizon turns to be

$$\dot{A}^2(w)Y(A(w)) + e^{-g(A(w))}V(A(w)) = 0, \quad (4.49)$$

where ϕ and g are represented as functions of A and only the leading terms are left. Similarly, we come from the full $3d$ dynamical system (2.48)-(2.50) to eqs.(4.14)-(4.15) with Y tending to infinity. Substituting into eq. (4.49) Y and g given by (4.16) and (4.48), respectively, we come to

$$\dot{A}^2(w) \frac{1}{A(w) - A_h} + V(A(w))e^{-c_g} \frac{1}{A(w) - A_h} = 0. \quad (4.50)$$

Taking into account the scale factor (4.47) the latter equation is brought to

$$\frac{1}{\left(\frac{(\Lambda^{(h)})^2}{a^2}w + c_A\right)^2} + V(A(w))e^{-c_g} = 0. \quad (4.51)$$

Since we are looking for a near-horizon solution, only two terms from eq.(2.21) dominate in eq.(4.50)). Expanding in series eq.(4.51) near w_h , we get

$$\frac{1}{\left(\frac{(\Lambda^{(h)})^2}{a^2}w_h + c_A\right)^2} \left(1 - \frac{2}{a^2} \frac{(\Lambda^{(h)})^2}{\left(\frac{(\Lambda^{(h)})^2}{a^2}w + c_A\right)^2} (w - w_h) \dots \right) = e^{-c_g} |V(\phi_h)| \left(1 - \frac{2}{a^2} \frac{(\Lambda^{(h)})^2}{\left(\frac{(\Lambda^{(h)})^2}{a^2}w + c_A\right)^2} (w - w_h) \dots \right), \quad (4.52)$$

where we use the definition of the parameters (4.38) and the solution for the scalar field (4.40)-(4.41). Finally, we find for c_g

$$c_g = \ln \left(|V(\phi_h)| \left(c_A + \frac{(\Lambda^{(h)})^2}{a^2} w_h \right)^2 \right) \quad (4.53)$$

or taking into account (4.38), (4.46) we can represent (4.53) as follows

$$c_g = \ln \left(2 + \frac{a^2}{\sqrt{2}} \frac{|V_\phi(\phi_h)|^2}{|V(\phi_h)|^{3/2}} w_h + \frac{a^4}{16} \frac{|V_\phi(\phi_h)|^4}{|V(\phi_h)|^3} w_h^2 \right), \quad (4.54)$$

from which one can see that choosing ϕ_h as $\phi_h = \phi_{1,2,3}$, the constant c_g turns to be $c_g = \ln 2$ as for the near-horizon metric of the AdS black hole (B.23).

Therefore, the blackening function f is given by

$$f = \frac{a^2 c_g}{(\Lambda^{(h)})^2} \ln \left(\frac{\frac{(\Lambda^{(h)})^2}{a^2} w + c_A}{\frac{(\Lambda^{(h)})^2}{a^2} w_h + c_A} \right), \quad (4.55)$$

where c_g is defined by (4.53). The black hole solution near the horizon is given by

$$ds^2 \simeq \left(\frac{\frac{(\Lambda^{(h)})^2}{a^2} w + c_A}{c_A} \right)^{\frac{2a^2}{(\Lambda^{(h)})^2}} (-f dt^2 + dx^2) + \frac{dw^2}{f}, \quad (4.56)$$

with f given by (4.55), and the scalar field by (4.40) with (4.41). It is interesting to note that the near-horizon solutions (4.56), (4.40), which we have constructed, have scaling geometries similar to those considered in [43].

5 Improved near-horizon solutions for the scalar field

In this section we will present a sketch how to find analytic solutions for asymptotically AdS black holes using additional conditions, which allow to construct a solution for the scalar field $\phi(A)$, defined for both near-horizon and near the boundary regions unlike the solution (4.39).

Imposing the constraint $X^2 \sim 0$ for the original equations (2.48)-(2.50) we are brought to the following system of equations

$$\frac{dz}{dA} = z(z-1)X, \quad (5.1)$$

$$\frac{dX}{dA} = -(Y+2)(X + \mathcal{C}_{(z,a)}), \quad (5.2)$$

$$\frac{dY}{dA} = -Y(Y+2). \quad (5.3)$$

The system (5.1)-(5.3) can also be mapped into a unit cylinder, so the solutions to it will almost coincide with the flows⁷ described in Figs. 8 and 10. It is interesting to note that for

⁷Now we are mainly interested in flows ending in p_1 .

the case $0 < a^2 < 1/2$ the solutions to eqs. (5.1)-(5.3) in the unit cylinder, which start with some ϕ_h and end in the critical point p_1 have a greater deviation from the trajectories in Fig. 8, which also end in p_1 , the further from $z = 1/2$ (i.e. the extremum of $V(\phi)$ at the origin) the initial condition is chosen. This happens due to the fact that the corresponding flows deviate more from $x = 0$.

Let us now consider the solution of the system (5.1)-(5.3) under the condition $Y(0) \rightarrow \infty$. The equation (5.3) is independent and has the following solution (see (B.3), also we take $A_h = 0$ for simplicity)

$$Y(A) = \frac{2}{e^{2A} - 1}. \quad (5.4)$$

Substituting the solution (5.4) into eq.(5.2) we come to

$$\frac{d\phi}{dA} = X, \quad (5.5)$$

$$\frac{dX}{dA} = -(1 + \coth A) \left(X + \frac{a^2 V_\phi(\phi)}{2 V(\phi)} \right), \quad (5.6)$$

where as in the previous section it is convenient to return from z to the original variable ϕ (2.38). Eqs. (5.5)-(5.6) are reduced to a single second-order differential equation

$$\frac{d^2\phi}{dA^2} + (1 + \coth A) \left(\frac{d\phi}{dA} + \frac{a^2 V_\phi(\phi)}{2 V(\phi)} \right) = 0, \quad (5.7)$$

It worth to be noted that the equation (4.19) for the scalar field from the previous section it is just expansion of eq.(5.7) by small A up to first order. Next, expanding eq.(5.7) near ϕ_h and doing some algebra, we get the equation

$$\tanh A \frac{d^2\Phi}{dA^2} + (\tanh A + 1) \left(\frac{d\Phi}{dA} + \mathbf{K}^{(h)}\Phi \right) = 0, \quad (5.8)$$

where we introduce the following quantity

$$\Phi := \phi - \phi_h + \frac{\Lambda^{(h)}}{\mathbf{K}^{(h)}} \quad (5.9)$$

with $\Lambda^{(h)}$ and $\mathbf{K}^{(h)}$ defined by (4.38). Eq.(5.8) with the transformation

$$r = e^{2A} \quad (5.10)$$

can be yielded to the form

$$r(1-r) \frac{d^2\Phi(r)}{dr^2} + (1-2r) \frac{d\Phi(r)}{dr} - \frac{\mathbf{K}^{(h)}}{2} \Phi(r) = 0. \quad (5.11)$$

The latter is a hypergeometric equation whose regular singular points $r = 1$ and $r = \infty$ correspond to the near-horizon and boundary regions, respectively.⁸ One of the fundamental solutions of eq. (5.11) near $r = 1$ can be represented in the form

$$\Phi(r) = {}_2F_1(a_h, 1 - a_h, 1, 1 - r), \quad (5.12)$$

⁸Recall that the scale factor A tending to 0 is related with a solution near the horizon, while $A \rightarrow \infty$ is associated with a solution near the boundary.

where the parameter a_h is defined as follows

$$a_h = \frac{1}{2} \left(1 - \sqrt{1 - 2\mathbf{K}^{(h)}} \right). \quad (5.13)$$

One can check that the solution for the scalar field (5.9) with (5.12) is related with the branch of solutions (4.39) given by Bessel functions of the first kind. This follows from the expansions

$$J_0 \left(2\sqrt{\mathbf{K}^{(h)}A} \right) = 1 - \mathbf{K}^{(h)}A + \left(\frac{\mathbf{K}^{(h)}A}{2} \right)^2 - \left(\frac{\mathbf{K}^{(h)}A}{6} \right)^3 + \dots \quad (5.14)$$

$${}_2F_1(a_h, 1 - a_h, 1, 1 - e^{2A}) = 1 - \mathbf{K}^{(h)}A + \left(\frac{\mathbf{K}^{(h)}A}{2} \right)^2 - \left(\frac{\mathbf{K}^{(h)}A}{6} \right)^3 \left(\frac{\mathbf{K}^{(h)} + 2}{\mathbf{K}^{(h)}} \right) + \dots$$

We should make some remarks regarding the limits of applicability of the equation (5.8). This equation corresponds to the system (5.1)-(5.3), for which the function $\mathcal{C}_{(z,a)}$ is expanded in series by z near z_h up to the first order. The flows associated with the simplified system (5.1)-(5.3) in the unit cylinder under the initial conditions of type (3.24) almost perfectly coincide with the flows in Fig. 10 but only if $z_h \sim z_1$; in other cases, there will be a good match as long as $y \neq 0$.

It should be noted that the equation (5.11) is very similar to the equation for the holographic two-point function for the holographic model (2.6) from [33] (up to the evolution parameter).

6 Conclusions

In this work we have considered holographic RG flows at finite temperature in $D = 3$ $\mathcal{N} = 2$ gauged supergravity coupled to a sigma model. Depending on the parameter a^2 related to the curvature of the target space, the scalar potential of the holographic model can have either a single ($0 < a^2 \leq \frac{1}{2}$) or three extrema ($\frac{1}{2} < a^2 < 1$) giving rise to AdS solutions, which are dual to CFTs.

We have represented the equations of motion of the holographic model as the autonomous dynamical system. Certain trajectories of the system can be interpreted as RG flows, while equilibria of the system correspond to fixed points of RG flow at zero temperature. Because of the black hole ansatz for the metric the dynamical system has infinite points corresponding to the near-horizon regions. By virtue of the Poincaré transformations we have projected the system into the unit cylinder, so the near-horizon regions mapped onto the critical line on the boundary of the cylinder.

We have numerically solved the equations of the system in the cylinder and plotted the global phase portraits. The flows starting from the near-horizon regions to the spacetime boundaries with various ϕ_h have been found numerically. Using the autonomous dynamical system helps to understand the behavior of the trajectories based on the stability analysis of fixed points. For the potential with a single extremum asymptotically AdS black hole solutions with any value of ϕ_h pass close to the exact RG flow, which is a separatrix, and end in the AdS fixed point, see Fig. 8. For the potential with a three extrema, the separatrices

are RG flows between AdS fixed points, corresponding to different extrema of the scalar potential, which were constructed numerically in [33,35], see Fig. 11. We have observed that black hole solutions, for which the value of ϕ_h is close to one of the additional extrema of the potential $\phi_{2,3}$, can end either at the AdS fixed point related with these extrema ($\phi_h = \phi_{2,3}$) or at the AdS fixed point associated with the maximum of the potential ($\phi_h \neq \phi_{2,3}$), see Fig. 10. Another type of solutions, which we have seen setting ϕ_h near the additional extrema $\phi_{2,3}$, are naked singularities.

We have found an analytic description of asymptotically AdS black holes for the near-horizon region. The constructed near-horizon geometries are scaling and defined by the value of the scalar field at the horizon ϕ_h . For ϕ_h coinciding with one of the extrema of the scalar potential the solution reproduce the metric of the AdS black hole near the horizon.

To extend the analytic black hole solutions to the boundary we have used additional constraints for the dynamical equations. This has led us to a hypergeometric equation for the scalar field on the scale factor. Regular singularities of the solution correspond to the near-horizon limit or near the boundary.

Despite we have considered a very special three-dimensional holographic model with the certain scalar potential, the method of construction and analysis of RG flows at finite temperature can be generalized to an arbitrary dimensions similarly to [23,24] as long as we consider black hole generalizations of Poincaré invariant domain wall solutions.

A natural continuation of this work is to find the full solutions of asymptotically AdS black holes from the horizon to the boundary, next, using them, to explore in details thermodynamical properties of RG flows .

Acknowledgements

We are grateful to Irina Ya. Aref'eva and Nikolay Tyurin for helpful discussions. We thank Eric Gourgoulhon for collaboration at the initial stages of this work. A.G. is grateful to the Paris Observatory, LUTH for warm hospitality, where a part of this work was done. The work of A.G. presented in Sections 2, 4 was supported by Russian Science Foundation grant RSCF-22-72-10122. The work of M.P. was supported by the JINR AYSS Foundation, Project No 24-301-03.

A Exact holographic RG flow

For the model (2.6) the exact domain wall solution, which preserve half of supersymmetries exists and was obtained in the work [33]. The scale factor of this solution reads

$$A_{\text{susy}} = \frac{1}{4a^2} \ln(e^{4a^2w} - 1), \quad (\text{A.1})$$

the scalar field is given by

$$\phi_{\text{susy}} = \frac{1}{2} \ln \left(1 + \frac{e^{-2a^2w}}{1 - e^{-2a^2w}} \right), \quad (\text{A.2})$$

where the radial coordinate w runs from 0 to ∞ .

The metric of the domain wall solution with (A.1) can be represented as follows

$$ds_{\text{susy}}^2 = \left(e^{4a^2w} - 1 \right)^{\frac{1}{2a^2}} (-dt^2 + dx^2) + dw^2. \quad (\text{A.3})$$

The domain wall solution (A.3) with (A.2) has an AdS asymptotics with $w \rightarrow \infty$, while if one send w to zero, the solution has a singular geometry. For $a^2 \leq \frac{1}{2}$ this singular behaviour turns to be acceptable since the solution satisfies the Gubser's bound.

B AdS black hole solutions

B.1 Exact solutions

Before analyzing the general case, we show that we are able to reconstruct an AdS black hole solution (2.26) from a solution of the autonomous system (2.48)-(2.50). Setting the scalar field to be constant $\phi = \phi_h$ (it can be $\phi_1 = 0$ or $\phi_{2,3}$ from (2.10)) and assuming that the scale factor $A \neq \text{const}$, it follows from (2.37)-(2.38) that $X = 0$ and $Z = \text{const}$.

Then the system (2.48)-(2.50) is reduced to the one equation on Y

$$\frac{dY}{dA} = -Y(Y + 2). \quad (\text{B.1})$$

To solve eq.(B.1) we impose the initial condition

$$Y(A_h) = \delta, \quad (\text{B.2})$$

with $A_h = A(w_h)$, $\delta > 0$, that leads to the following solution

$$Y(A) = \frac{2\delta}{(\delta + 2)e^{2(A-A_h)} - \delta}. \quad (\text{B.3})$$

Considering the limit $\delta \rightarrow \infty$ in (B.3), we obtain

$$Y(A) = \frac{2}{e^{2(A-A_h)} - 1}. \quad (\text{B.4})$$

Substituting (B.4) into the relation for Y (2.37) and integrating the resulting expression, we find the *log* of the blackening function f , i.e. $g(A)$:

$$g = c_g + \ln(1 - e^{-2(A-A_h)}), \quad (\text{B.5})$$

where c_g is a constant of integration.

One can find a solution to A in terms of w integrating the equation

$$\ddot{A} = 0, \quad (\text{B.6})$$

that immediately gives

$$A = c_A w + c_w. \quad (\text{B.7})$$

The latter integration constant c_w in (B.7) can be set to 0 due to the equations of motion are invariant under shift of the radial coordinate w . As for c_A we can derive it plugging back (B.5),(B.7) into any of the Einstein equations (2.21)-(2.23), so

$$c_A = e^{-c_g/2} \sqrt{-\frac{V(\phi_h)}{2}}. \quad (\text{B.8})$$

The constant c_g can be find taking into account that the blackening function f on the boundary should tend to 1. Thus, c_g is fixed as

$$c_g = 0. \quad (\text{B.9})$$

Note, that the condition that f goes to 0 on the horizon is also satisfied with (B.5). Finally, the metric functions look like

$$A = \sqrt{-\frac{V(\phi_h)}{2}} w, \quad f = 1 - e^{-\sqrt{-2V(\phi_h)}(w-w_h)}, \quad (\text{B.10})$$

that is in agreement with (2.26).

We also show how to find a near-horizon asymptotic solution using the reduced dynamical system below. For certain choice of integration constants we see matching between the exact and asymptotic solutions.

B.2 Near-horizon solutions

Next, we will demonstrate, using as an example eq. (B.1), how to recover gravitational solutions that matches to solutions of a corresponding dynamical system near its infinite critical points.

For (B.1) we find two finite equilibrium points

$$Y = 0, \quad Y = -2. \quad (\text{B.11})$$

To analyze the system at infinity we map (B.1) to $1d$ disc \mathbf{D} , using transformation

$$Y = \frac{\tilde{Y}}{\sqrt{1 - \tilde{Y}^2}}, \quad (\text{B.12})$$

Then the dynamical system (B.1) on the disc looks like

$$\frac{d\tilde{Y}}{dA} = -\tilde{Y} \left(\tilde{Y} \sqrt{1 - \tilde{Y}^2} + 2(1 - \tilde{Y}^2) \right). \quad (\text{B.13})$$

The critical points corresponding to (B.13) are

$$\tilde{Y} = 0, \quad \tilde{Y} = -\frac{2}{\sqrt{5}}, \quad \tilde{Y} = -1, \quad \tilde{Y} = 1. \quad (\text{B.14})$$

Two additional points $\tilde{Y} = \pm 1$ correspond to $Y = \pm\infty$. Note that the exact solutions indicated in the previous subsection correspond to the solution connecting the critical point $\tilde{Y} = 1$ with the critical point $\tilde{Y} = 0$.

To find an asymptotic solution to eq.(B.13) near the equilibrium point $\tilde{Y} = 1$, we introduce a new variable ϵ_y , so that

$$\tilde{Y} = 1 - \epsilon_y, \quad (\text{B.15})$$

where $0 < \epsilon_y \ll 1$. Substituting (B.15) into (B.13) and removing higher order terms, we get

$$\frac{d\epsilon_y(A)}{dA} \simeq \sqrt{2\epsilon_y(A)}, \quad (\text{B.16})$$

where we used that ϵ is small.

Solving equation (B.16) with the boundary condition $\epsilon_y(A_h) = \delta$ and then sending δ to zero we find

$$\epsilon_y(A) \simeq \frac{1}{2}(A - A_h)^2. \quad (\text{B.17})$$

Doing the inverse transformations (B.15) and (B.12), we obtain

$$Y \simeq \frac{1}{A - A_h} - \frac{1}{2}(A - A_h), \quad (\text{B.18})$$

where $A \gtrsim A_h$. Remembering the definition of Y from the second relation of (2.37) we find the corresponding function $g(A)$

$$g(A) \simeq c_g + \ln(A - A_h), \quad (\text{B.19})$$

where c_g is a constant of integration. So we have for the blackening function f

$$f(A) \simeq e^{c_g}(A - A_h). \quad (\text{B.20})$$

To reconstruct the function $A(w)$, we use the Einstein equations setting the scalar field to be constant. Subtracting (2.21) from (2.23) and taking into account $\phi_h = \phi(w_h)$, we obtain the equation for A

$$\ddot{A} = 0. \quad (\text{B.21})$$

Then the scale factor A takes the form as in the previous subsection (B.7) $A = c_A w$. One can determine the constants c_A , c_g by substitution of the solutions for A and g into any

of the equations of motion (2.21)-(2.23) such that only the terms of higher order survive. Finally, we have for them

$$c_A = e^{-c_g/2} \sqrt{-V(\phi_h)}. \quad (\text{B.22})$$

Note that the relation for c_A differs by a factor $\frac{1}{\sqrt{2}}$ comparing to the explicit case (B.8). Thus, to reach matching the solutions we should set c_g as follows

$$c_g = \ln 2. \quad (\text{B.23})$$

Thus we obtain the following formula for the blackening function near the horizon

$$f \simeq \sqrt{-2V(\phi_h)}(w - w_h). \quad (\text{B.24})$$

Note, that in this case the solution (B.24) is just an expansion of the solution (2.26) near the horizon.

C Fixed points and holographic RG flows at $T = 0$

C.1 Stability of the critical points

Here we discuss stability of the critical points of (3.15)-(3.17) in sense of the 3d dynamical system. We summarize the types of stability for each of the point in Table.2

| | $0 < a^2 < \frac{1}{2}$ | $a^2 = \frac{1}{2}$ | $\frac{1}{2} < a^2 < 1$ | $a^2 = 1$ | $a^2 > 1$ |
|--------------------|------------------------------|---------------------|-------------------------|----------------|-----------|
| p_1 | stable node | | | non-hyperbolic | saddle |
| $p_{2,3}$ | — | | saddle | — | |
| $p_{4,7}$ | saddle | — | unstable node | | |
| $p_{5,9}, p_{6,8}$ | non-hyperbolic, non-isolated | | | | |
| $q_{1,2}$ | — | saddle | — | | |
| $g_{1,3}$ | saddle* | | | | |
| $g_{2,4}$ | stable node* | | | | |

Table 2: Classification of critical points of the dynamical system (3.15)-(3.17).

Here the non-hyperbolic means that one of eigenvalues equals to zero, non-isolated means that this point lies on the critical curve. However, if we fix $y = 0$, that is, we consider the invariant manifold xz -plane, then non-isolated points become isolated and the classification obtained in the works [34,35] is valid for them. The asterisk means that one of the eigenvalues is not defined; but it turns out to be defined in any arbitrarily small neighborhood of these points. The absolute value of this eigenvalue, of course, depends on the neighborhood, but its sign is always uniquely determined. This makes it possible to identify the nature of the stability of these points (saddle, stable node), which was also verified by numerical construction of flows near these points.

C.2 Holographic RG flows at zero temperature

Let's list possible holographic RG flows for different choices of a^2 :

1. $0 < a^2 < \frac{1}{2}$
 - (a) from p_1 (CFT₁ **UV**) at $\phi_{*1} = 0$ to p_4 , with $\phi \rightarrow +\infty$, triggered by a relevant operator (Dirichlet b.c.),
 - (b) from p_1 (CFT₁ **UV**) at $\phi_{*1} = 0$ to p_4 , with $\phi \rightarrow +\infty$, triggered by a relevant operator (Neumann b.c.),
 - (c) from CFT₁ **UV** p_1 at ϕ_{*1} to p_5 , with $\phi \rightarrow +\infty$, driven by a non-zero vacuum expectation value of the scalar operator (Dirichlet b.c.),
 - (d) from CFT₁ **UV** p_1 at ϕ_{*1} to p_5 , with $\phi \rightarrow +\infty$, driven by a non-zero vacuum expectation value of the scalar operator (Neumann b.c.);
2. $a^2 = \frac{1}{2}$
 - (a) from p_1 (CFT₁ **UV**) at $\phi_{*1} = 0$ to p_5 , with $\phi \rightarrow +\infty$, triggered by a non-zero vacuum expectation value of the scalar operator (Dirichlet b.c.);
 - (b) from p_1 (CFT₁ **UV**) at $\phi_{*1} = 0$ to p_4 , with $\phi \rightarrow +\infty$, triggered by a source (Neumann b.c.);
 - (c) from p_1 (CFT₁ **UV**) at $\phi_{*1} = 0$ to q_1 , with $\phi \rightarrow +\infty$, triggered by a single trace operator (Dirichlet b.c.),
 - (d) from p_1 (CFT₁ **UV**) at $\phi_{*1} = 0$ to q_1 , with $\phi \rightarrow +\infty$, triggered by a non-vanishing VEV (Neumann b.c.);
3. $\frac{1}{2} < a^2 < 1$
 - (a) from p_1 (CFT₁ **UV**) at $\phi_{*1} = 0$ to p_4 , with $\phi \rightarrow +\infty$, triggered by a source (Dirichlet b.c.)
 - (b) from p_1 (CFT₁ **UV**) at $\phi_{*1} = 0$ to p_4 , with $\phi \rightarrow +\infty$, triggered by a VEV of the operator (Neumann b.c.)
 - (c) from p_1 (CFT₁ **UV**) to p_2 (CFT₂ **IR**), driven by a source (Dirichlet b.c.)
 - (d) from p_1 (CFT₁ **UV**) to p_2 (CFT₂ **IR**), driven by a non-zero VEV (Neumann b.c., Mixed b.c)
 - (e) from p_1 (CFT₁ **UV**) to p_3 (CFT₃ **IR**), driven by a source (Dirichlet b.c.)
 - (f) from p_1 (CFT₁ **UV**) to p_3 (CFT₃ **IR**), driven by a non-zero VEV (Neumann b.c., Mixed b.c)

References

- [1] M. Gell-Mann and F. E. Low, Quantum electrodynamics at small distances, *Phys. Rev. D*, **95** (1954) 1300–1312.
- [2] N. N. Bogolyubov and D.V. Shirkov, “ Charge renormalization group in quantum field theory,” *Nuovo Cim.*, **3** (1956) 845–863.
- [3] N. N. Bogolyubov and D. V. Shirkov, “Introduction to the Theory of Quantized Fields,” *Interscience Monographs* **3** (1959).
- [4] K. Symanzik, ”Small distance behavior in field theory and power counting”, *Commun. Math. Phys.*, **18**, 227–246, (1970).
- [5] Jr. Callan, G.Curtis, ”Broken scale invariance and asymptotic behavior”, *Phys. Rev. D*, **5** (1972) 3202–3210.
- [6] K. G. Wilson and J. B. Kogut, “The Renormalization group and the epsilon expansion,” *Phys. Rept.* **12** (1974) 75-199.
- [7] J. M. Maldacena, “The Large N limit of superconformal field theories and supergravity,” *Adv. Theor. Math. Phys.* **2** (1998), 231-252; [arXiv:hep-th/9711200].
- [8] E. Witten, “Anti-de Sitter space and holography,” *Adv. Theor. Math. Phys.* **2** (1998), 253-291, [arXiv:hep-th/9802150].
- [9] S. S. Gubser, I. R. Klebanov and A. M. Polyakov, “Gauge theory correlators from noncritical string theory,” *Phys. Lett. B* **428** (1998), 105-114; [arXiv:hep-th/9802109].
- [10] I. Y. Aref’eva and I. V. Volovich, “On large N conformal theories, field theories in anti-de Sitter space and singletons,” [arXiv:hep-th/9803028].
- [11] E. T. Akhmedov, “A Remark on the AdS / CFT correspondence and the renormalization group flow,” *Phys. Lett. B* **442** (1998), 152-158; [arXiv:hep-th/9806217].
- [12] J. de Boer, E. P. Verlinde and H. L. Verlinde, “On the holographic renormalization group,” *JHEP* **08** (2000), 003, [arXiv:hep-th/9912012].
- [13] D. Z. Freedman, S. S. Gubser, K. Pilch and N. P. Warner, Renormalization group flows from holography supersymmetry and a c-theorem, *Adv. Theor. Math. Phys.* **3**(1999) 363; [arXiv:hep-th/9904017].
- [14] S. de Haro, S. N. Solodukhin and K. Skenderis, “Holographic reconstruction of space-time and renormalization in the AdS / CFT correspondence,” *Commun. Math. Phys.* **217** (2001), 595-622; [arXiv:hep-th/0002230].
- [15] J. de Boer, The Holographic renormalization group, *Fortsch. Phys.* **49**, 339 (2001); [arXiv:hep-th/0101026].

- [16] M. Bianchi, D.Z. Freedman and K. Skenderis, Holographic renormalization, *Nucl. Phys.* **B 631** (2002) 159; [arXiv:hep-th/0112119].
- [17] M. Bianchi, D. Z. Freedman and K. Skenderis, “How to go with an RG flow,” *JHEP* **08** (2001), 041; [arXiv:hep-th/0105276].
- [18] K. Skenderis, ”Lecture notes on holographic renormalization,” *Class. Quant. Grav.* **19** (2002), 5849-5876; [arXiv:hep-th/0209067].
- [19] I. Papadimitriou and K. Skenderis, “AdS / CFT correspondence and geometry,” *IRMA Lect. Math. Theor. Phys.* **8** (2005), 73-101; [arXiv:hep-th/0404176].
- [20] I. Papadimitriou and K. Skenderis, “Correlation functions in holographic RG flows,” *JHEP* **10** (2004), 075; [arXiv:hep-th/0407071].
- [21] I. Papadimitriou, “Multi-Trace Deformations in AdS/CFT: Exploring the Vacuum Structure of the Deformed CFT,” *JHEP* **05** (2007), 075; [arXiv:hep-th/0703152].
- [22] S. S. Gubser, “Curvature singularities: The Good, the bad, and the naked,” *Adv. Theor. Math. Phys.* **4** (2000), 679-745; [arXiv:hep-th/0002160].
- [23] E. Kiritsis, F. Nitti and L. Silva Pimenta, “Exotic RG Flows from Holography,” *Fortsch. Phys.* **65** (2017) no.2, 1600120; [arXiv:1611.05493[hep-th]].
- [24] U. Gürsoy, E. Kiritsis, F. Nitti and L. Silva Pimenta, “Exotic holographic RG flows at finite temperature,” *JHEP* **10**, 173 (2018); [arXiv:1805.01769[hep-th]].
- [25] Y. Bea and D. Mateos, “Heating up Exotic RG Flows with Holography,” *JHEP* **08**, 034 (2018); [arXiv:1805.01806[hep-th]].
- [26] U. Gursoy, E. Kiritsis, L. Mazzanti and F. Nitti, “Holography and Thermodynamics of 5D Dilaton-gravity,” *JHEP* **05** (2009), 033; [arXiv:0812.0792[hep-th]].
- [27] I. Aref’eva and K. Rannu, “Holographic Anisotropic Background with Confinement-Deconfinement Phase Transition,” *JHEP* **05**, 206 (2018); [arXiv:1802.05652[hep-th]].
- [28] I. Ya. Aref’eva, A.A. Golubtsova and G. Policastro, Exact holographic RG flows and the $A_1 \times A_1$ Toda chain, *JHEP* 05 (2019) **117**; [arXiv:1803.06764[hep-th]].
- [29] I. Ya. Aref’eva, Holographic Renormalization Group Flows, *Theor. Math. Phys.* **200**, 1313–1323 (2019).
- [30] I. Ya. Aref’eva, K. Rannu, Holographic renormalization group flow in anisotropic matter, *Theoret. and Math. Phys.*, **202:2** (2020), 272–283.
- [31] I. Y. Aref’eva, A. Hajilou, P. Slepov and M. Usova, “Running Coupling and Beta-Functions for HQCD with Heavy and Light Quarks,” [arXiv:2402.14512[hep-th]].
- [32] N. S. Deger, A. Kaya, E. Sezgin and P. Sundell, Matter coupled AdS3 supergravities and their black strings, *Nucl. Phys.* **B 573** (2000) 275, [arXiv:hep-th/9908089].

- [33] N. S. Deger, Renormalization group flows from $D = 3$, $N=2$ matter coupled gauged supergravities, *JHEP* **11** (2002), 025; [[arXiv:hep-th/0209188](#)].
- [34] A. A. Golubtsova and M. K. Usova, “Stability analysis of holographic RG flows in 3d supergravity,” *Eur. Phys. J. Plus* **138**, no.3, 260 (2023); [[arXiv:2208.01179](#) [[hep-th](#)]].
- [35] K. Arkhipova, L. Astrakhantsev, N. S. Deger, A. A. Golubtsova, K. Gubarev, E. T. Musaev, Holographic RG flows and boundary conditions in a 3D gauged supergravity, [[arXiv:2402.11586](#) [[hep-th](#)]].
- [36] S. Gukov, RG Flows and Bifurcations, *Nucl.Phys.* **B 919** (2017) 583-638; [[arXiv:1608.06638](#) [[hep-th](#)]].
- [37] I. Arav, K. C. M. Cheung, J. P. Gauntlett, M. M. Roberts and C. Rosen, “Superconformal RG interfaces in holography,” *JHEP* **11** (2020), 168; [[arXiv:2007.07891](#) [[hep-th](#)]].
- [38] S. Lefschetz, Differential Equations: Geometric Theory Pure and applied mathematics, California University, 1962.
- [39] L. Perko, Differential Equations and Dynamical Systems. Texts in Applied Mathematics 7, Berlin, 2001.
- [40] N. N. Bautin and E. A. Leontovich, Methods and Ways of Qualitative Study of Dynamic Systems on a Plane,” In Russian, Nauka, Moscow, 1976.
- [41] A. Ganguly, R. Gannouji, R. Goswami and S. Ray, Global structure of black holes via the dynamical system, *Class. Quant. Grav.* **32** (2015) no.10, 105006; [[arXiv:1411.2601](#) [[gr-qc](#)]].
- [42] M. Cruz, A. Ganguly, R. Gannouji, G. Leon and E. N. Saridakis, “Global structure of static spherically symmetric solutions surrounded by quintessence,” *Class. Quant. Grav.* **34** (2017) no.12, 125014; [[arXiv:1702.01754](#) [[gr-qc](#)]].
- [43] K. Goldstein, S. Kachru, S. Prakash and S. P. Trivedi, “Holography of Charged Dilaton Black Holes,” *JHEP* **08** (2010), 078; [[arXiv:0911.3586](#) [[hep-th](#)]].
- [44] S. Wiggins, Introduction to Applied Nonlinear Dynamical Systems and Chaos, *Springer*, New York (2003).